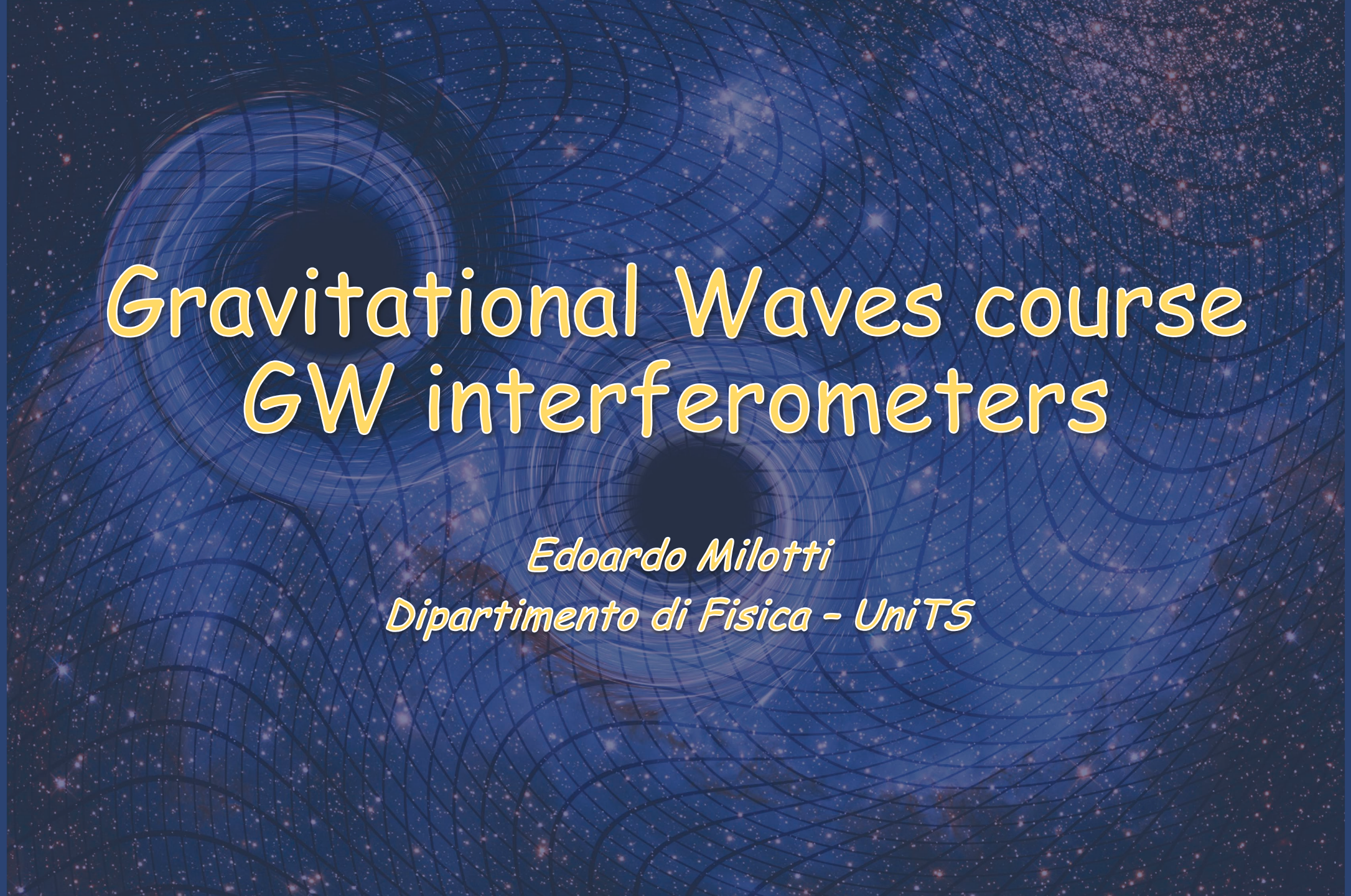

Gravitational Waves course
GW interferometers

Edoardo Milotti
Dipartimento di Fisica - UniTS

VIRGO

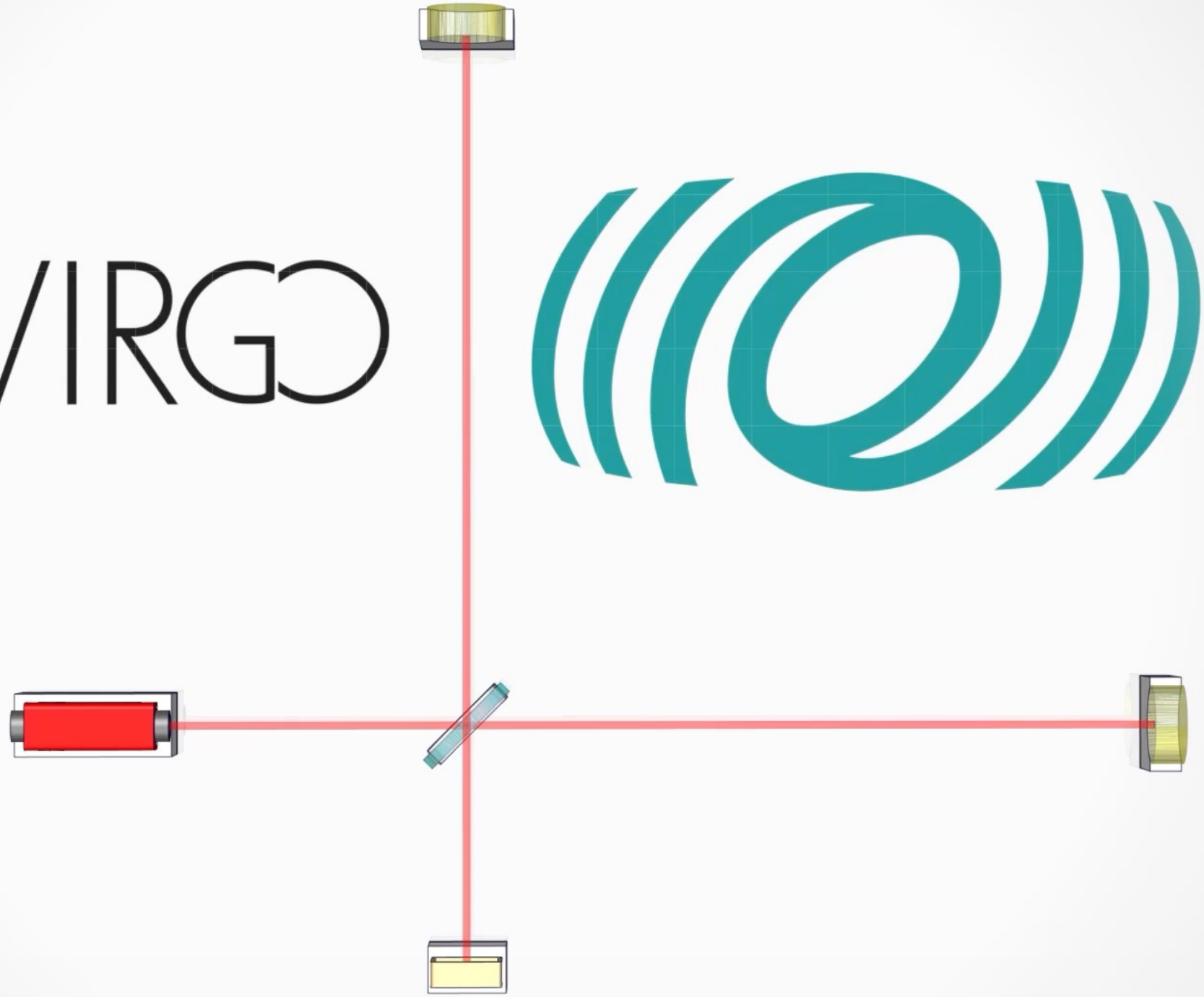

Michelson interferometers

(the main reference for these slides is the paper by Black and Gutenkunst, *An introduction to signal extraction in interferometric gravitational wave detectors*, Am. J. Phys. **71** (2003) 365)

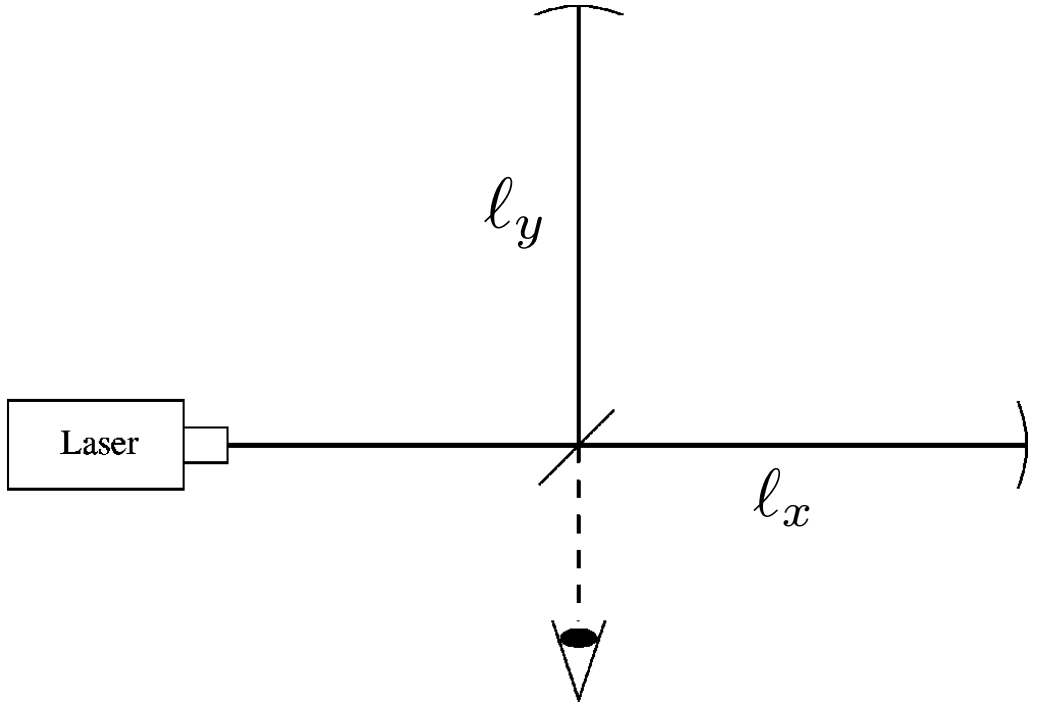

Fig. 2. A basic Michelson interferometer is sensitive to the kinds of strain a gravitational wave will produce. Incident laser light is split by a beam splitter, sent down orthogonal paths along the x and y axis, reflected from mirrors at the ends of these paths, and recombined back at the beam splitter. The interference between these two return beams produces a net intensity that is sensitive to differential changes in the lengths of the arms.

$$
\begin{aligned}
E_{\rm out} &= \frac{1}{2}\left(r_x e^{ik(2\ell_x)} - r_y e^{ik(2\ell_y)}\right) E_{\rm in} \\
&\rightarrow \quad -\frac{1}{2}\left(e^{ik(2\ell_x)} - e^{ik(2\ell_y)}\right) E_{\rm in} \\
&= -\frac{1}{2} e^{ik(\ell_x+\ell_y)}\left(e^{ik(\ell_x-\ell_y)} - e^{-ik(\ell_x-\ell_y)}\right) E_{\rm in} \\
&= -ie^{ik(\ell_x+\ell_y)} \sin\left[k(\ell_x-\ell_y)\right] E_{\rm in}
\end{aligned}
$$

(note that the amplitude reflection coefficients are equal to -1 for a perfect mirror; moreover in this formula we consider the substrate of the beamsplitter where the reflection picks up an additional minus sign *only in one direction of propagation*)

$$P \propto \left\langle |E|^2 \right\rangle \quad \Rightarrow \quad P_{\rm out} = \sin^2\left[k(\ell_x-\ell_y)\right] P_{\rm in}$$

Transfer function

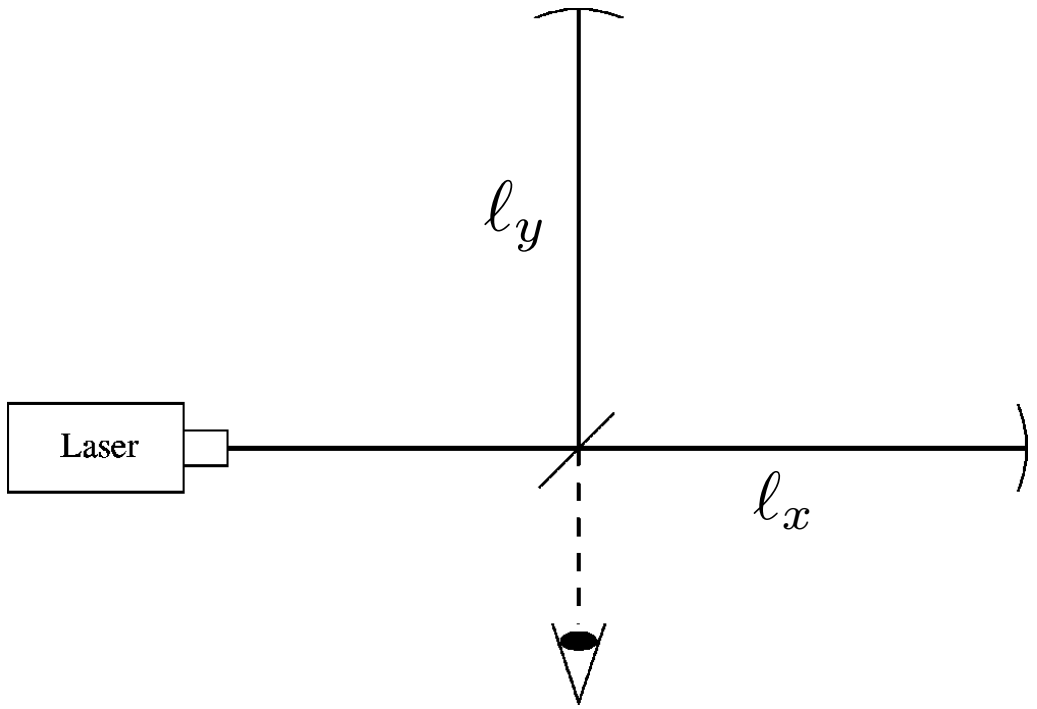

Fig. 2. A basic Michelson interferometer is sensitive to the kinds of strain a gravitational wave will produce. Incident laser light is split by a beam splitter, sent down orthogonal paths along the x and y axis, reflected from mirrors at the ends of these paths, and recombined back at the beam splitter. The interference between these two return beams produces a net intensity that is sensitive to differential changes in the lengths of the arms.

The ratio of the electric field amplitudes

$$H(\omega) = \frac{E_{\rm out}}{E_{\rm in}} = -ie^{ik(\ell_x+\ell_y)} \sin\left[k(\ell_x - \ell_y)\right]$$

$$\text{where } k = \omega/c$$

is the *transfer function* of the interferometer.

Effect of a GW with + polarization (w.r.t. the interferometer arms)

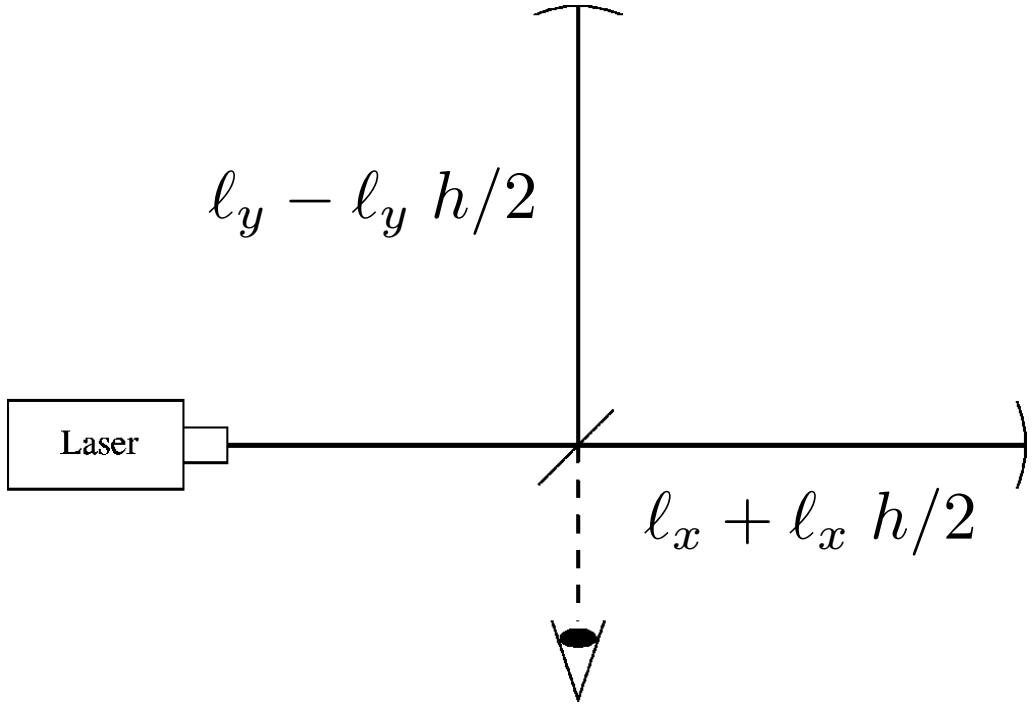

Fig. 2. A basic Michelson interferometer is sensitive to the kinds of strain a gravitational wave will produce. Incident laser light is split by a beam splitter, sent down orthogonal paths along the x and y axis, reflected from mirrors at the ends of these paths, and recombined back at the beam splitter. The interference between these two return beams produces a net intensity that is sensitive to differential changes in the lengths of the arms.

$$(\ell_x + \ell_x\ h/2) - (\ell_y - \ell_y\ h/2) \approx \delta\ell + \ell h$$

$$\text{where} \quad \ell = \frac{\ell_x + \ell_y}{2}; \quad \delta\ell = \ell_x - \ell_y$$

$$\Rightarrow \quad P_{\rm out} = \cos^2\left[k(\delta\ell + \ell h)\right] P_{\rm in}$$

and the transfer function becomes

$$H(\omega) = e^{2ik\ell} \cos\left[k(\delta\ell + \ell h)\right]$$

Effect of a GW with + polarization (w.r.t. the interferometer arms)

$$P_{\rm out} = \cos^2\left[k(\delta\ell + \ell h)\right] P_{\rm in}$$

$$\approx P_{\rm in}\cos^2\left(k\delta\ell\right) P_{\rm in} + P_{\rm in}\left(\frac{d}{du}\cos^2 u\Big|_{k\delta\ell}\right) k\ell h + \frac{1}{2}P_{\rm in}\left(\frac{d^2}{du^2}\cos^2 u\Big|_{k\delta\ell}\right) k^2\ell^2 h^2$$

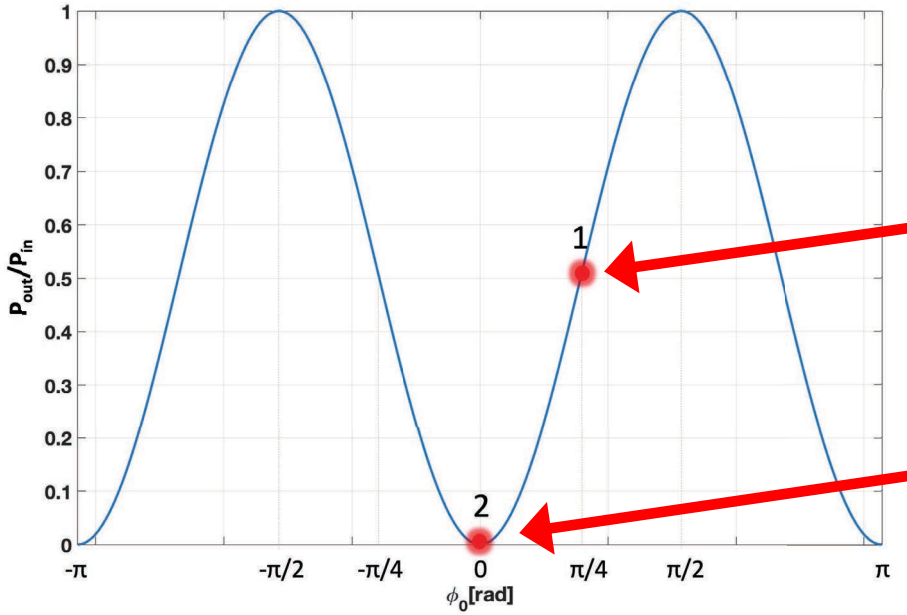

$$P_{\rm out} \approx \frac{P_{\rm in}}{2}(1 - 2k\ell h)$$ linear

$$P_{\rm out} \approx P_{\rm in}\, k^2\ell^2 h^2$$ quadratic

Fig. 3. The intensity of the light at the observation port versus the difference in arm lengths (units of λ, the wavelength of the light). Operating at point 1 maximizes the change in power for a given change in arm lengths, but also makes the instrument sensitive to intensity noise in the light source. Operating at point 2 eliminates this problem, but, in a simple Michelson interferometer, it reduces the signal to a second-order effect.

"2" is the *null point* of the interferometer

Phase modulation

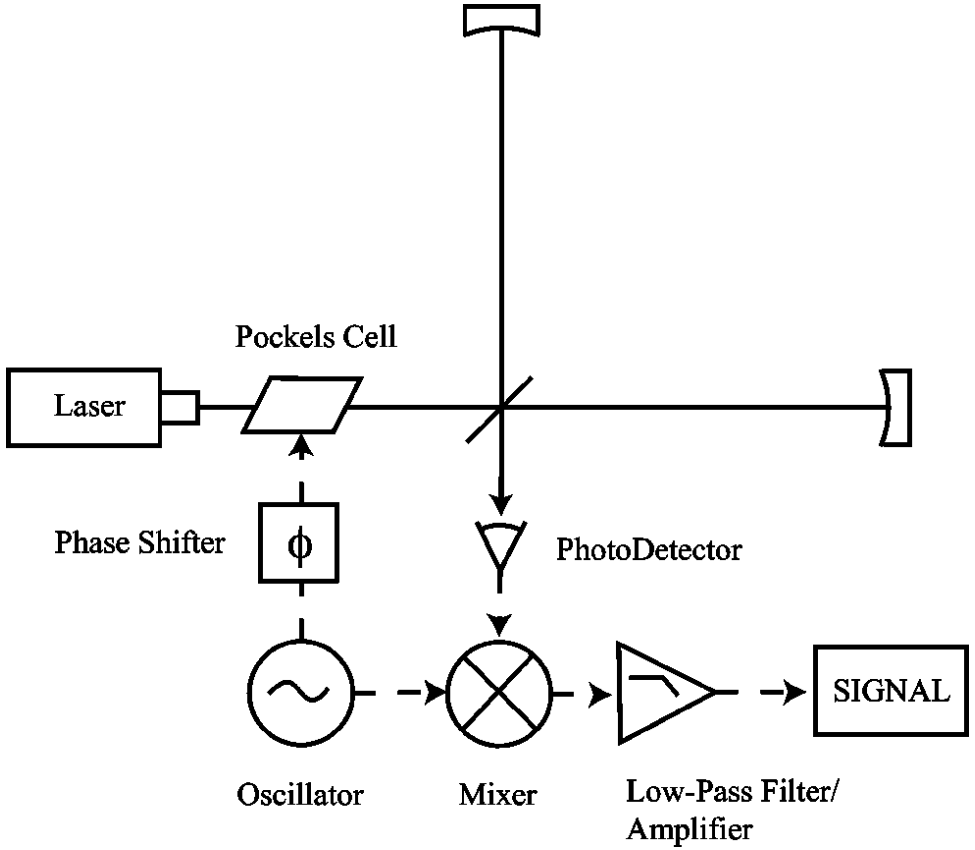

Fig. 6. We can use lock-in detection to recover a linear signal from a dark port.

We use phase modulation to linearize the interferometer response at the null point

$$E_{\text{in}} = E_0 e^{i(\omega t + \beta \sin \Omega t)} \quad (\omega = ck)$$

Mathematical aside:

Bessel's functions of the first kind and integer order

Consider Laplace's equation in cylindrical coordinates

$$\nabla^2\Phi = 0$$

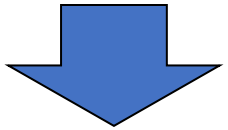

$$\nabla^2\Phi = \frac{\partial^2\Phi}{\partial r^2} + \frac{1}{r}\frac{\partial\Phi}{\partial r} + \frac{1}{r^2}\frac{\partial^2\Phi}{\partial\theta^2} + \frac{\partial^2\Phi}{\partial z^2} = 0$$

we try a factored solution

$$\Phi(r,\theta,z) = R(r)\Theta(\theta)Z(z)$$

then, we obtain

$$\frac{\partial^2 R}{\partial r^2}\Theta(\theta)Z(z)+\frac{1}{r}\frac{\partial R}{\partial r}\Theta(\theta)Z(z)+\frac{1}{r^2}\frac{\partial^2 \Theta}{\partial \theta^2}R(r)Z(z)+\frac{\partial^2 Z}{\partial z^2}R(r)\Theta(\theta)=0$$

$$\left(\frac{1}{R}\frac{\partial^2 R}{\partial r^2}+\frac{1}{r}\frac{\partial R}{\partial r}\right)+\frac{1}{r^2}\left(\frac{1}{\Theta}\frac{\partial^2 \Theta}{\partial \theta^2}\right)+\left(\frac{1}{Z}\frac{\partial^2 Z}{\partial z^2}\right)=0$$

The last sum depends on three separate pieces that depend on different, independent variables, and the only way for it to hold for all values of the variables is that each piece is a constant.

$$\left(\frac{1}{R}\frac{\partial^2 R}{\partial r^2}+\frac{1}{r}\frac{\partial R}{\partial r}\right)+\frac{1}{r^2}\left(\frac{1}{\Theta}\frac{\partial^2 \Theta}{\partial \theta^2}\right)+\left(\frac{1}{Z}\frac{\partial^2 Z}{\partial z^2}\right)=0$$

$$\Rightarrow \quad \frac{1}{Z}\frac{\partial^2 Z}{\partial z^2}=\lambda^2$$

$$\Rightarrow \quad r^2\left(\frac{1}{R}\frac{\partial^2 R}{\partial r^2}+\frac{1}{r}\frac{\partial R}{\partial r}\right)+\left(\frac{1}{\Theta}\frac{\partial^2 \Theta}{\partial \theta^2}\right)=-\lambda^2 r^2$$

$$\Rightarrow \quad r^2\left(\frac{1}{R}\frac{\partial^2 R}{\partial r^2}+\frac{1}{r}\frac{\partial R}{\partial r}+\lambda^2\right)=-\frac{1}{\Theta}\frac{\partial^2 \Theta}{\partial \theta^2}=n^2$$

$$\Rightarrow \quad \frac{1}{\Theta}\frac{\partial^2 \Theta}{\partial \theta^2}=-n^2 \quad \text{and} \quad r^2\frac{\partial^2 R}{\partial r^2}+r\frac{\partial R}{\partial r}+\left(\lambda^2 r^2-n^2\right)R=0$$

The first two equations are easy to solve

$$\frac{\partial^2 Z}{\partial z^2} = \lambda^2 Z \quad \Rightarrow \quad Z(z) = A_\lambda e^{\lambda z} + B_\lambda e^{-\lambda z}$$

$$\frac{\partial^2 \Theta}{\partial \theta^2} = -n^2 \Theta \quad \Rightarrow \quad \Theta(\theta) = C_n \cos n\theta + D_n \sin n\theta$$

The third equation

$$x^2 \frac{\partial^2 R}{\partial x^2} + x \frac{\partial R}{\partial x} + \left(x^2 - n^2\right) R = 0 \qquad (x = \lambda r)$$

is **Bessel's equation of order *n***

Now let $J_n(x)$ be the solution of the n-th order equation, then

$$x^2 \frac{\partial^2 J_n}{\partial x^2} + x \frac{\partial J_n}{\partial x} + \left(x^2 - n^2\right) J_n = 0$$

and when we introduce the generating function

$$F(x,t) = \sum_{n=-\infty}^{+\infty} J_n(x) t^n$$

we find that it satisfies the equation

$$x^2 \frac{\partial^2 F}{\partial x^2} + x \frac{\partial F}{\partial x} + x^2 F = t^2 \frac{\partial^2 F}{\partial t^2} + t \frac{\partial F}{\partial t}$$

(prove it! For a solution, see the final slides)

The following function satisfies the p.d.e.

$$F(x,t)=\exp\left[\frac{x}{2}\left(t-\frac{1}{t}\right)\right]$$

which we can confirm by direct substitution into the equation.

Finally, if we let

$$t=e^{i\theta}$$

we find the **Jacobi-Anger identity**

$$F(x,\theta)=\exp\left[\frac{x}{2}\left(e^{i\theta}-e^{-i\theta}\right)\right]=\exp(ix\sin\theta)=\sum_n J_n(x)e^{in\theta}$$

Since the generating function

$$F(x,t)=\exp\left[\frac{x}{2}\left(t-\frac{1}{t}\right)\right]=\sum_n J_n(x)t^n$$

is invariant with respect with the exchange $t \leftrightarrow -1/t$ we also find

$$F(x,t)=\sum_n J_n(x)t^n=\sum_n(-1)^n J_n(x)t^{-n}=\sum_n(-1)^n J_{-n}(x)t^n$$

and therefore

$$J_n(x)=(-1)^n J_{-n}(x)$$

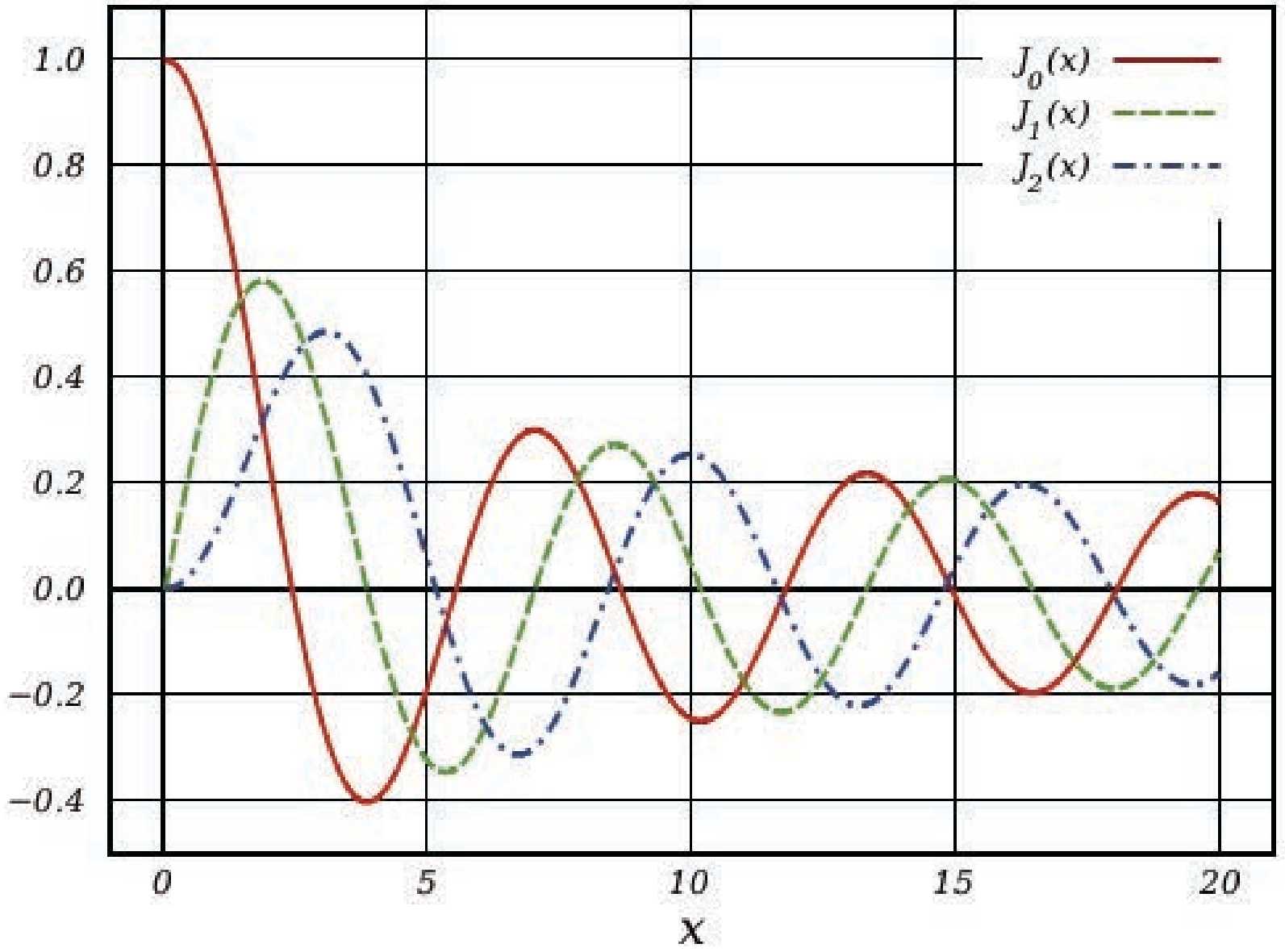
1.0
0.8
0.6
0.4
0.2
0.0
−0.2
−0.4
0
5
10
15
20
x
$J_0(x)$
$J_1(x)$
$J_2(x)$

Phase modulation

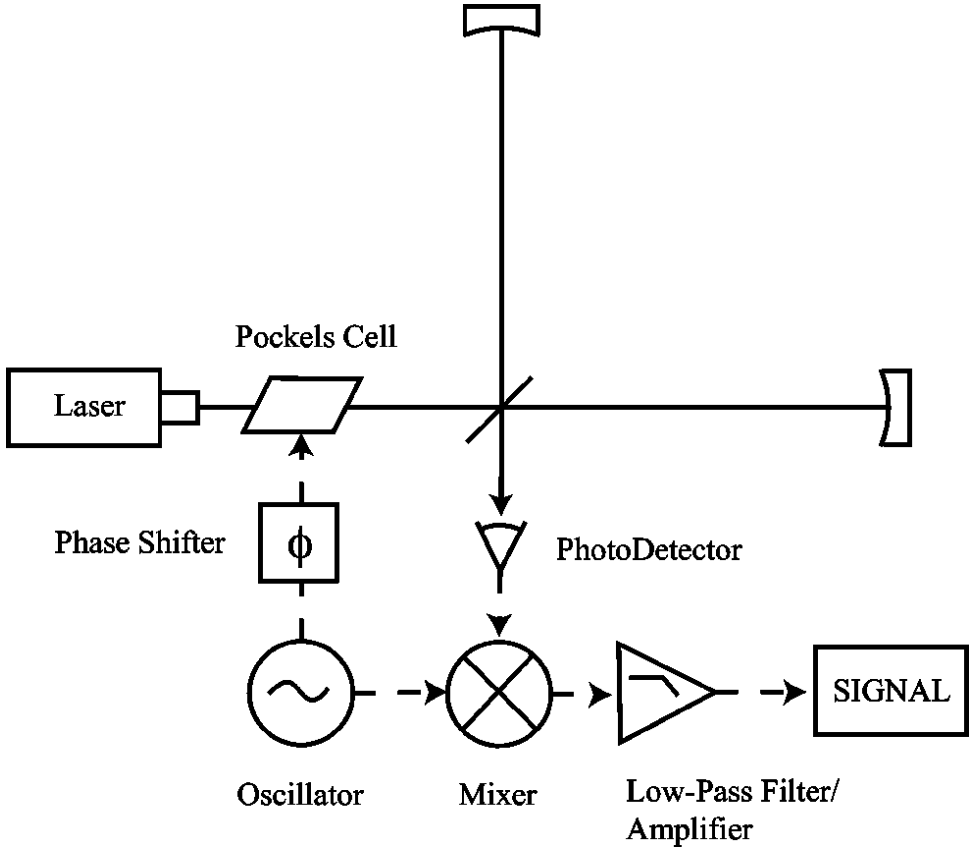

Fig. 6. We can use lock-in detection to recover a linear signal from a dark port.

modulation index

$$E_{\text{in}} = E_0 e^{i(\omega t + \beta \sin \Omega t)} \quad (\omega = ck)$$

since

$$e^{ix \sin \theta} = \sum_n J_n(x) e^{in\theta}$$

then

$$E_{\text{in}} \approx E_0 e^{i\omega t} \left(J_0(\beta) + J_1(\beta) e^{i\Omega t} - J_1(\beta) e^{-i\Omega t} \right)$$
$$= E_0 \left(J_0(\beta) e^{i\omega t} + J_1(\beta) e^{i(\omega+\Omega)t} - J_1(\beta) e^{i(\omega-\Omega)t} \right)$$

carrier

sidebands

Response of the interferometer

$$E_{\text{in}} = E_0 \left(J_0(\beta) e^{i\omega t} + J_1(\beta) e^{i(\omega+\Omega)t} - J_1(\beta) e^{i(\omega-\Omega)t} \right)$$

$$E_{\text{out}} = E_0 \left(H(\omega) J_0(\beta) e^{i\omega t} + H(\omega+\Omega) J_1(\beta) e^{i(\omega+\Omega)t} - H(\omega-\Omega) J_1(\beta) e^{i(\omega-\Omega)t} \right)$$

$$= E_0 \left(H_0 J_0(\beta) e^{i\omega t} + H_+ J_1(\beta) e^{i(\omega+\Omega)t} - H_- J_1(\beta) e^{i(\omega-\Omega)t} \right)$$

with wavenumbers $$k_\pm = \frac{\omega \pm \Omega}{c} = 2\pi \left(\frac{1}{\lambda} \pm \frac{1}{\lambda_{\text{modulation}}} \right)$$

We can make the arms unequal in length so that $\cos k\delta\ell = 1$ and therefore $\sin k\delta\ell = 0$
(the difference is the *Schnupp asymmetry*)

With the Schnupp asymmetry, the transfer function evaluated at the carrier frequency is

$$\begin{aligned} H_0 &= -ie^{2ik\ell}\sin\left[k(\delta\ell + \ell h)\right] \\ &\approx -ie^{2ik\ell}\left[\sin(k\delta\ell)\cos(k\ell h) + \cos(k\delta\ell)\sin(k\ell h)\right] \\ &\approx -ie^{2ik\ell}k\ell h = -ie^{2ik\ell}\frac{2\pi\ell}{\lambda}h \end{aligned}$$

while at the sideband frequencies we find

$$\begin{aligned} H_\pm &= -ie^{2ik\ell}\sin\left[k(\delta\ell + \ell h)\right] = -ie^{2i(\omega\pm\Omega)\ell/c}\sin\left[\frac{\omega\pm\Omega}{c}(\delta\ell + \ell h)\right] \\ &= -ie^{2i(\omega\pm\Omega)\ell/c}\left\{\sin\left[\frac{\omega}{c}(\delta\ell + \ell h)\right]\cos\left[\frac{\Omega}{c}(\delta\ell + \ell h)\right] \pm \cos\left[\frac{\omega}{c}(\delta\ell + \ell h)\right]\sin\left[\frac{\Omega}{c}(\delta\ell + \ell h)\right]\right\} \\ &\approx \mp ie^{2i(\omega\pm\Omega)\ell/c}\sin\left(\frac{\Omega}{c}\delta\ell\right) = \mp ie^{2ik\ell}\ e^{\pm 2i\Omega\ell/c}\sin\left(\frac{\Omega}{c}\delta\ell\right) \end{aligned}$$

Total electric field at the output port

$$
\begin{aligned}
E_{\text{out}} &= E_0 \left(H_0 J_0(\beta) e^{i\omega t} + H_+ J_1(\beta) e^{i(\omega+\Omega)t} - H_- J_1(\beta) e^{i(\omega-\Omega)t} \right) \\
&= -i\, E_{\text{in}} e^{2ik\ell} e^{i\omega t} \left[J_0(\beta) \frac{2\pi\ell}{\lambda} h + J_1(\beta) \sin\left(\frac{\Omega}{c}\delta\ell\right) \left(e^{i\Omega t + 2i\Omega\ell/c} + e^{-i\Omega t - 2i\Omega\ell/c} \right) \right] \\
&= -i\, E_{\text{in}} e^{2ik\ell} e^{i\omega t} \left[J_0(\beta) \frac{2\pi\ell}{\lambda} h + 2J_1(\beta) \sin\left(\frac{\Omega}{c}\delta\ell\right) \cos\left(\Omega t + 2\Omega\ell/c\right) \right]
\end{aligned}
$$

Total power at the output port

$$E_{\rm out} = -i\ E_{\rm in} e^{2ik\ell} e^{i\omega t} \left[J_0(\beta) \frac{2\pi\ell}{\lambda} h + 2J_1(\beta) \sin\left(\frac{\Omega}{c}\delta\ell\right) \cos\left(\Omega t + 2\Omega\ell/c\right) \right]$$

$$P_{\rm out} = P_{\rm in} \left[J_0^2(\beta) \frac{4\pi^2\ell^2}{\lambda^2} h^2 + 4J_1^2(\beta) \sin^2\left(\frac{\Omega}{c}\delta\ell\right) \cos^2\left(\Omega t + 2\Omega\ell/c\right) \right.$$
$$\left. + 4J_0(\beta) J_1(\beta) \sin\left(\frac{\Omega}{c}\delta\ell\right) \frac{2\pi\ell}{\lambda} h \cos\left(\Omega t + 2\Omega\ell/c\right) \right]$$

$$P_{\rm out} = P_{\rm in}\left[J_0^2(\beta)\frac{4\pi^2\ell^2}{\lambda^2}h^2 + 4J_1^2(\beta)\sin^2\left(\frac{\Omega}{c}\delta\ell\right)\cos^2\left(\Omega t + 2\Omega\ell/c\right)\right.$$
$$\left. +4J_0(\beta)J_1(\beta)\sin\left(\frac{\Omega}{c}\delta\ell\right)\frac{2\pi\ell}{\lambda}h\cos\left(\Omega t + 2\Omega\ell/c\right)\right]$$

recalling that $\cos^2\theta = \frac{1}{2}(1+\cos 2\theta)$ we find:

$$P_{\rm out} = P_{\rm in}\left[J_0^2(\beta)\frac{4\pi^2\ell^2}{\lambda^2}h^2 + 2J_1^2(\beta)\sin^2\left(\frac{\Omega}{c}\delta\ell\right)\right.$$
$$\left. +2J_1^2(\beta)\sin^2\left(\frac{\Omega}{c}\delta\ell\right)\cos\left(2\Omega t + 4\Omega\ell/c\right) + J_0(\beta)J_1(\beta)\sin\left(\frac{\Omega}{c}\delta\ell\right)\cos\left(\Omega t + 2\Omega\ell/c\right)\frac{8\pi\ell}{\lambda}h\right]$$

DC Fourier components

$$P_{\rm out} = P_{\rm in}\left[J_0^2(\beta)\frac{4\pi^2\ell^2}{\lambda^2}h^2 + 2J_1^2(\beta)\sin^2\left(\frac{\Omega}{c}\delta\ell\right)\right.$$

$$\left. +2J_1^2(\beta)\sin^2\left(\frac{\Omega}{c}\delta\ell\right)\cos\left(2\Omega t + 4\Omega\ell/c\right) + J_0(\beta)J_1(\beta)\sin\left(\frac{\Omega}{c}\delta\ell\right)\cos\left(\Omega t + 2\Omega\ell/c\right)\frac{8\pi\ell}{\lambda}h\right]$$

component at twice the modulation frequency, which does not carry useful information on wave amplitude

sideband power, linear in the wave amplitude

Photodiode response is proportional to power

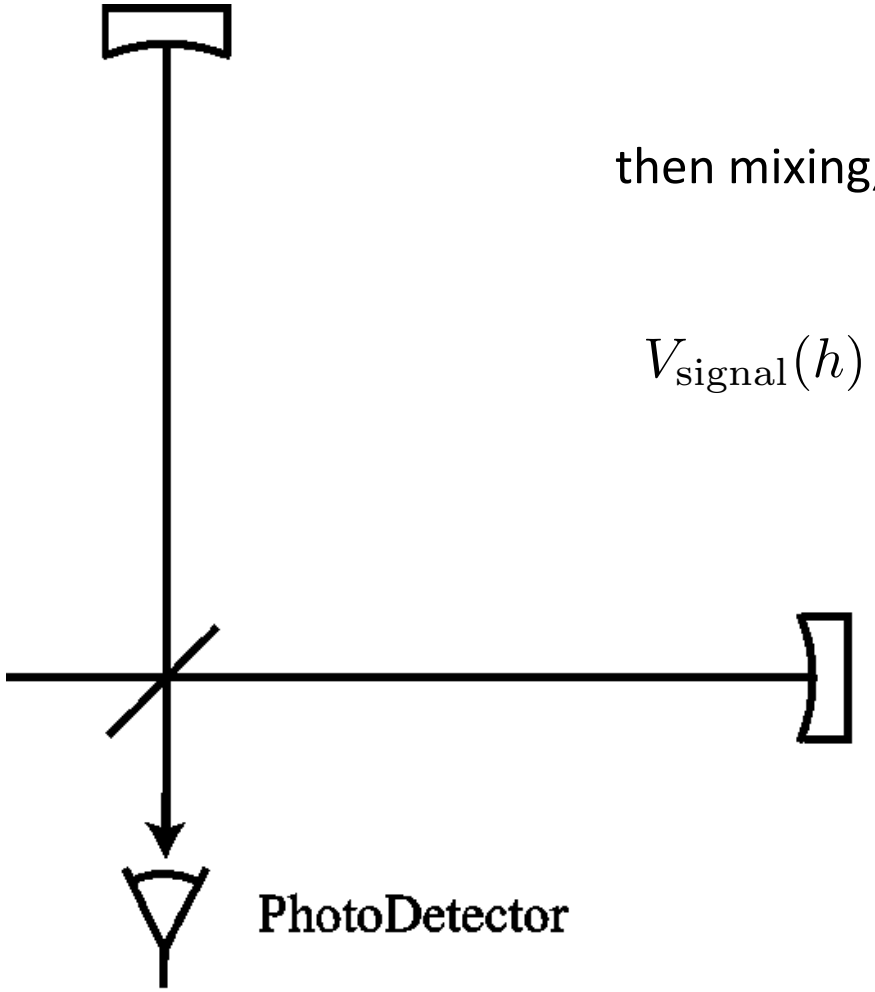

$$V_{\mathrm{PD}}(h) = RP_{\mathrm{out}}(h) = RJ_0(\beta)J_1(\beta)\sin\left(\frac{\Omega}{c}\delta\ell\right)\cos\left(\Omega t + 2\Omega\ell/c\right)\frac{8\pi\ell}{\lambda}h$$

then mixing, averaging, and adjusting phase to maximize the signal

$$V_{\mathrm{signal}}(h) = \langle V_{\mathrm{PD}}(h)\cos(\Omega t + \phi)\rangle = 2RJ_0(\beta)J_1(\beta)\sin\left(\frac{\Omega}{c}\delta\ell\right)\frac{2\pi\ell}{\lambda}h$$

the Schnupp asymmetry is chosen so that power is maximized in the signal-recycling cavity (see later), and in practice, for Virgo, this means that

$$\delta\ell = 23\ \mathrm{cm}$$

Virgo’s 35-cm diameter mirrors have an almost perfect surface

The large mirrors of Advanced Virgo are a crucial part of the detector. Indeed, achieving the best sensitivity to gravitational waves requires the loss of as little laser light as possible in the detector. For that purpose, all the three ingredients of a mirror, the substrate, the polishing and the coating, are at the frontier of current technology:

1. The substrate is made with the **purest glass in the world** (it is a synthetic quartz called “fused silica”). This glass has extremely low absorption and is homogeneous and uniform in all the directions. Despite its outstanding properties, it can come in relatively large size. For example, the mirror forming the 3-km arm cavities have a 350 mm diameter, are 200 mm thick, and have a mass of 40 kg.
2. The polishing, to shape the mirror profile, is done at the atomic level: on the central part of the mirror, the **largest defects on the surface have a height of just 5 atoms**.
3. The last step, the coating, is made to have reflective mirrors. The coating is precisely tuned so that the mirror has the desired reflectivity at the operational wavelength and so that **less than 0.0001% of the laser light is lost when it is reflected by the mirror** (due to the absorption, residual transmission, or scattering). This precise coating is done with a unique machine located in a laboratory of the Virgo Collaboration in the Lyon metropolitan area (LMA, Laboratoire des Matériaux Avancés). The mirrors for the LIGO interferometers are also coated in this laboratory.

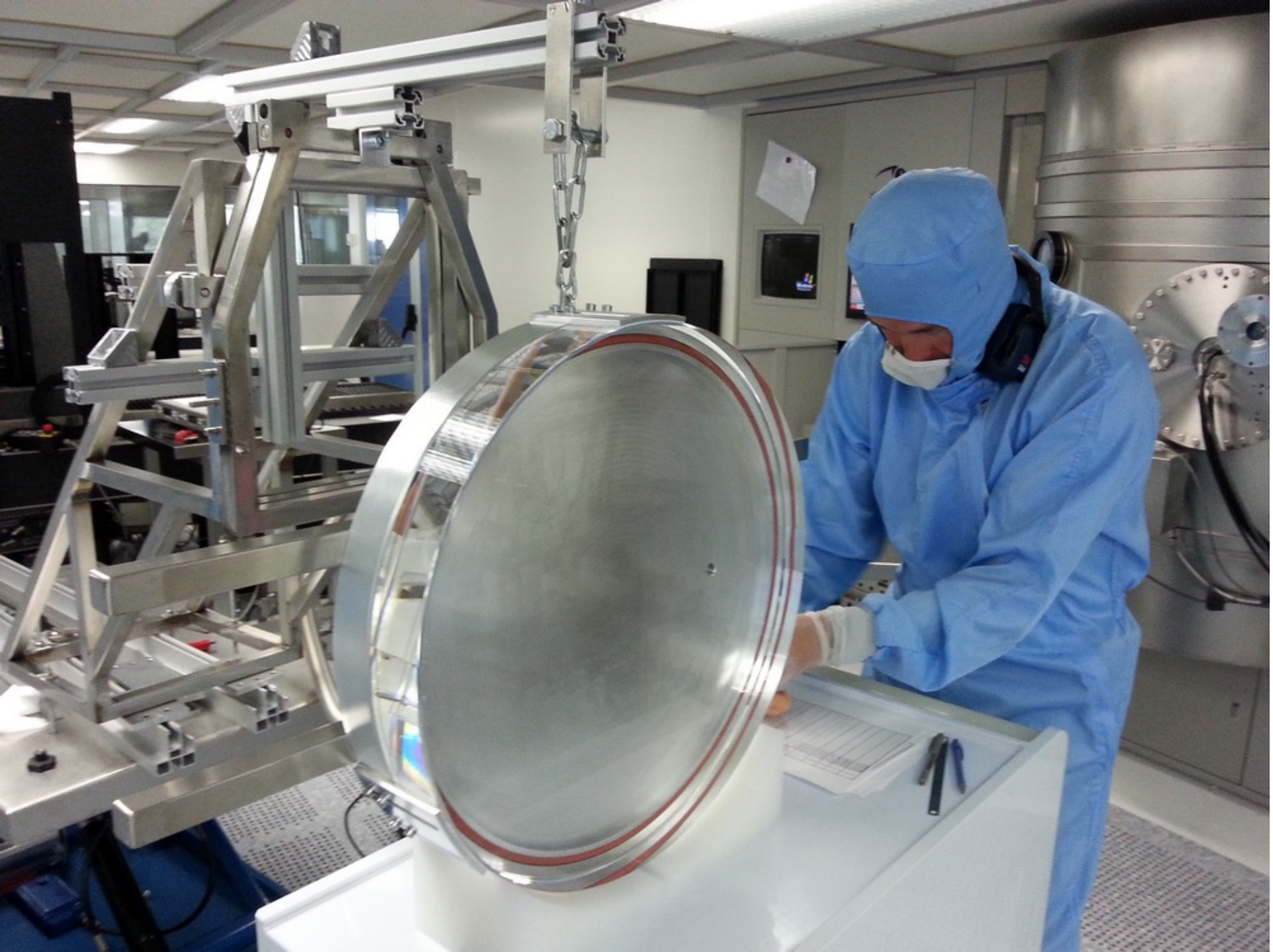

Picture of the Advanced Virgo beam-splitter mirror (diameter 550 millimeters) being prepared in the LMA clean room.

Credit: Virgo Collaboration/LMA/L. Pinard

The two Advanced Virgo end mirrors after they have been coated at LMA.

Credits: Virgo collaboration/LMA/L. Pinard

Virgo’s 40 kg mirrors are suspended by thin glass wires

Because of their non-zero temperature, atoms and molecules of mirrors and suspension wires are vibrating: these induce vibrations of the mirror surface that may mimic a gravitational wave passing the interferometer. The way the large mirrors of Advanced Virgo are suspended is thus crucial to reduce this thermal noise.

For that purpose, **suspensions wires made of the same glass (fused silica) as the mirrors have been developed to minimize the pendulum thermal noise of suspended mirrors**.

These suspensions are called *monolithic* since the wires are welded to the mirrors and are both composed of the same fused silica. This design allows to reduce the friction at the mirror-wire contact point, which is a source of the thermal noise. With the *monolithic* choice, the dissipations are so low that pendulum oscillations in vacuum can last for months before stopping. Moreover, fused silica wires have a high breaking strength, about twice that of steel wires. Such strength is very important, since the suspension must be highly resistant to the mechanical stress caused by oscillations of the mirror itself and to possible mechanical shocks of the mirror onto the surrounding materials.

The material of the suspension must be precisely controlled and produced, and carefully manipulated. For this reason, the **glass fibers (diameter of 0.4 mm and length of 0.7 m) are directly produced in the laboratories in Cascina** using a laser machine and tested with very high accuracy and reproducibility.

A particular **chemical bonding technique (silicate bonding) has also been developed to join all the glass components in a unique element**. This kind of suspension is apparently very fragile, but instead it is highly resistant along the fiber direction. However, special care must be taken to prevent any possible lateral damage to the fibers themselves.

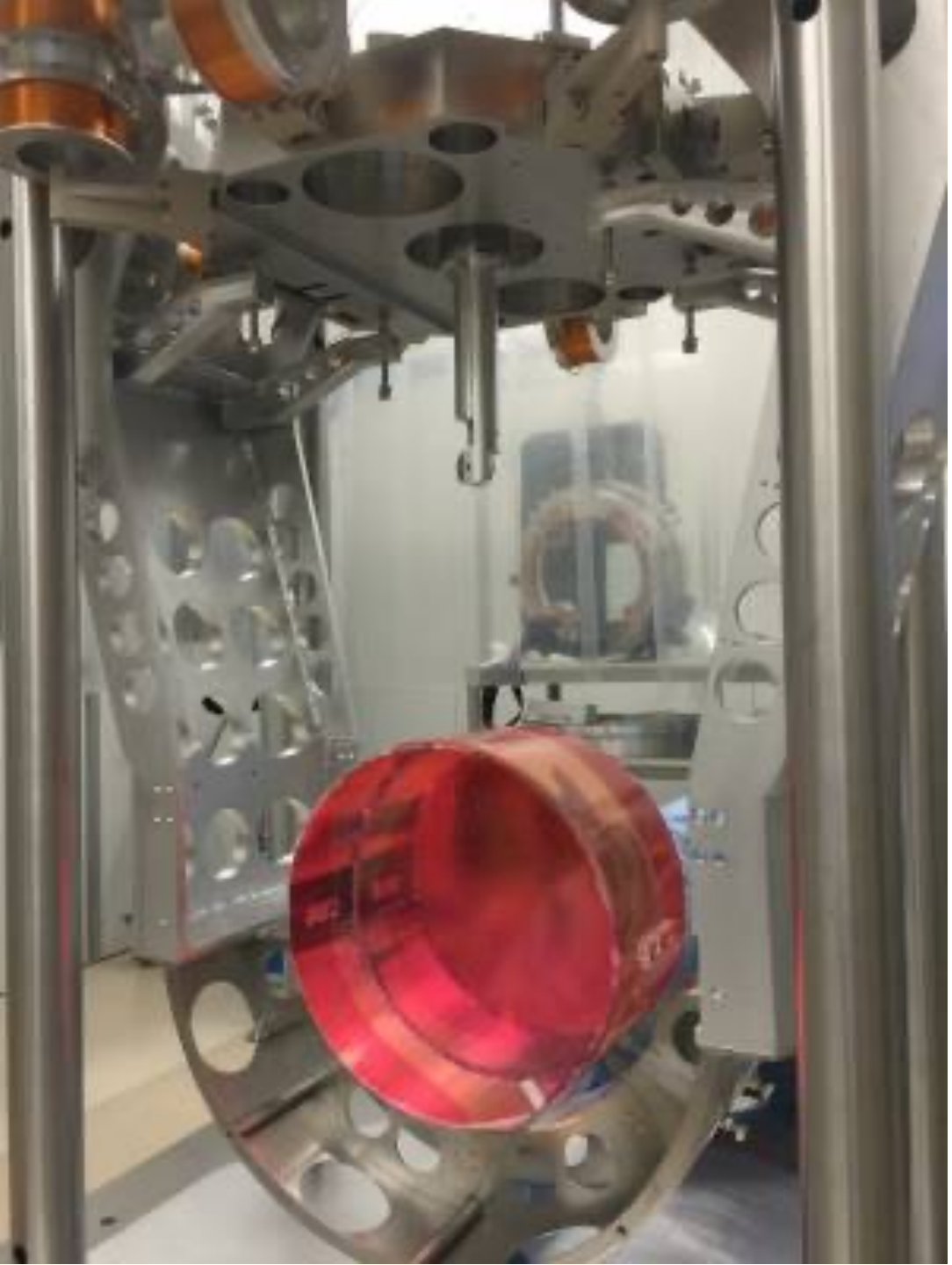

42 kg mirror (with a thin pink protecting film) suspended inside the payload by two thin wires of fused silica (glass).

Credits: Virgo collaboration

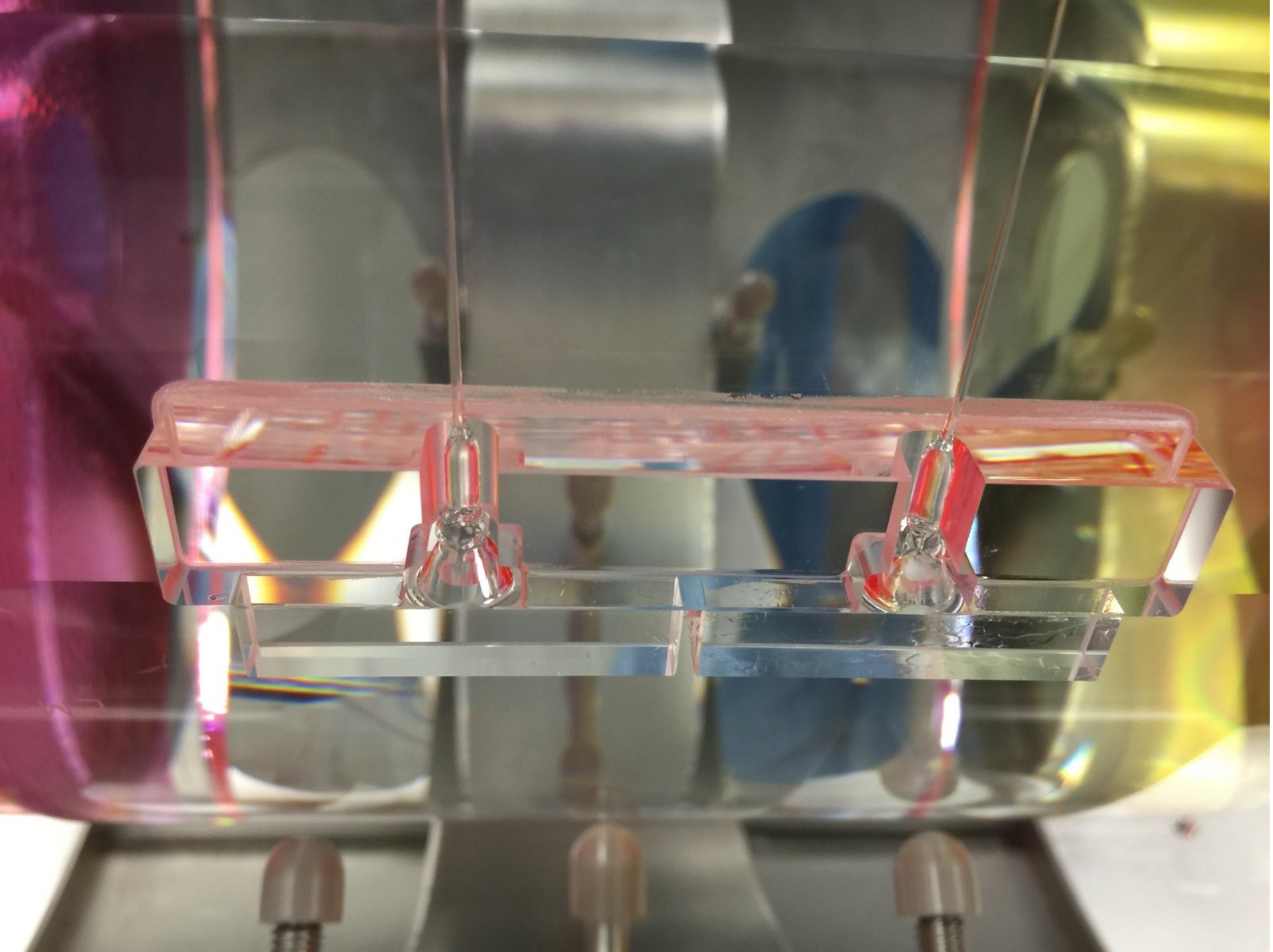

Zoom on an anchor bonded to one side of a mirror and attached monolithically to two thin fused silica wires used to suspend the 42 kg mirror.

Credits: Virgo collaboration

Virgo is a kilometer-wide optical table suspended and placed in ultra-high vacuum

The Virgo interferometer is a huge optical table placed under ultra-high vacuum. Each optical element is suspended with a seismic isolation system that is housed in a vacuum tank.

Two types of suspensions have been developed. **The interferometer mirrors and the main optical benches are suspended with the so-called "super-attenuators", housed in vacuum "towers"** about 10-m high. For Advanced Virgo, **five more optical benches sensing the interferometer beams have been suspended with the so-called "multi-stage seismic attenuation system" and housed in vacuum "mini-towers"** more than 3 meters high.

The vacuum towers are linked together by vacuum tubes for the passage of the laser beams. The largest tubes of Virgo, that link the two towers of the Fabry-Perot cavities are 3 km long and 1.2 m diameter. This makes Virgo a huge ultra-high vacuum chamber of 6800 m^3.

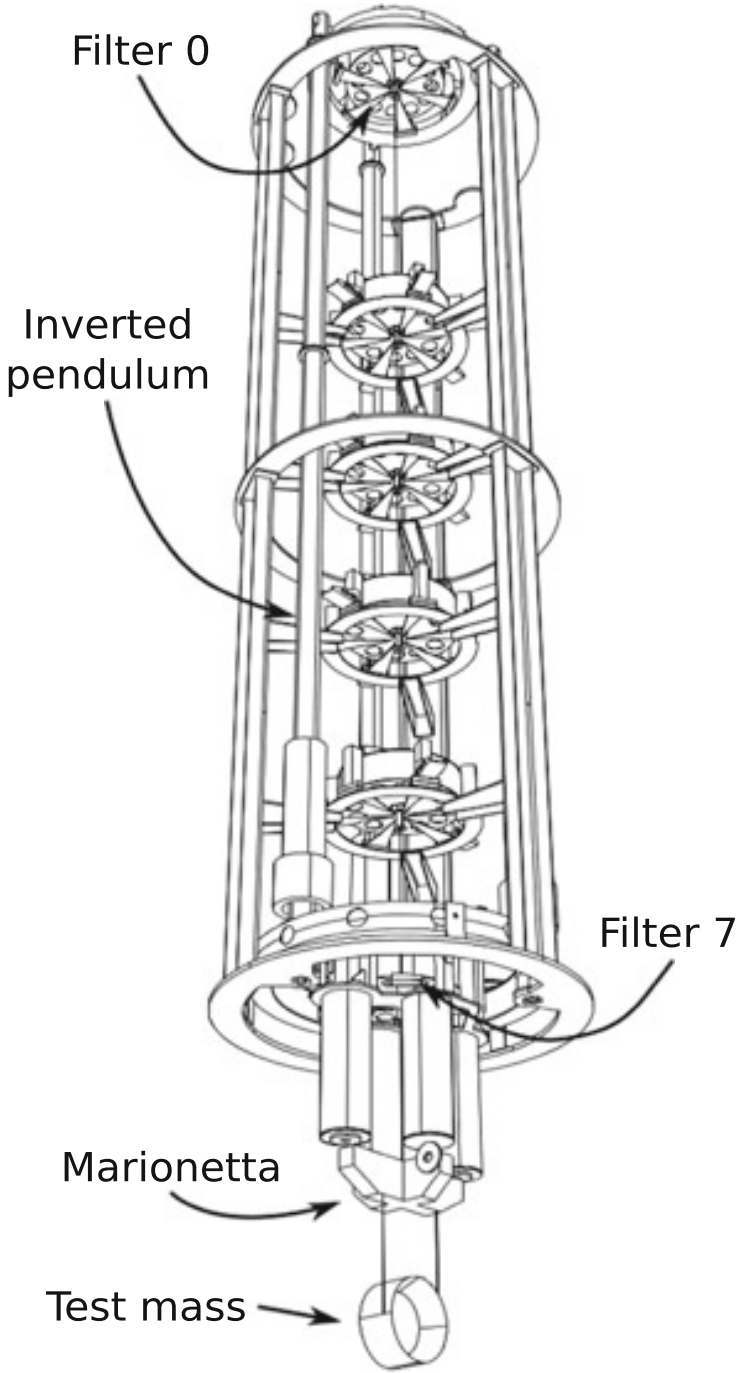

Ultra-high vacuum in the large tubes and around the mirrors is crucial for two reasons. Moving residual air molecules would hit the mirrors, inducing tiny displacements of the mirrors; moreover, the laser beam would interact with the air molecules, modifying its path and loosing power. That would perturb the measurement of gravitational waves. Therefore, the path of the light beam that travels in each Fabry-Perot cavity has to be evacuated down to the extremely low pressure of 10^{-12} atmospheres (100 times lower than for initial Virgo).

To attain this very low value, special metallurgical processes such as hydrogen desorption at 400°C have been developed for the fabrication of the vacuum parts. In addition, to eliminate the water vapor in the large 3-km long tubes, they will be heated at 150°C for one month each and cryogenic traps have been installed for Advanced Virgo at each end of the tubes to stop the migration of water molecules from the unbaked towers to the tubes. Despite their thermal isolation, each 3-km vacuum tube requires a power close to 1 MW to perform the heating operation.

The optical benches host a lot of mirrors, lenses and sensors (photodiodes and cameras). In Virgo, these optical elements were slightly vibrating because of ground vibrations and environmental sounds. This was limiting the Virgo sensitivity to gravitational waves.

In order to attenuate these vibrations, the new Advanced Virgo benches, weighting about 320 kg, have been suspended and placed into vacuum like the large mirrors.

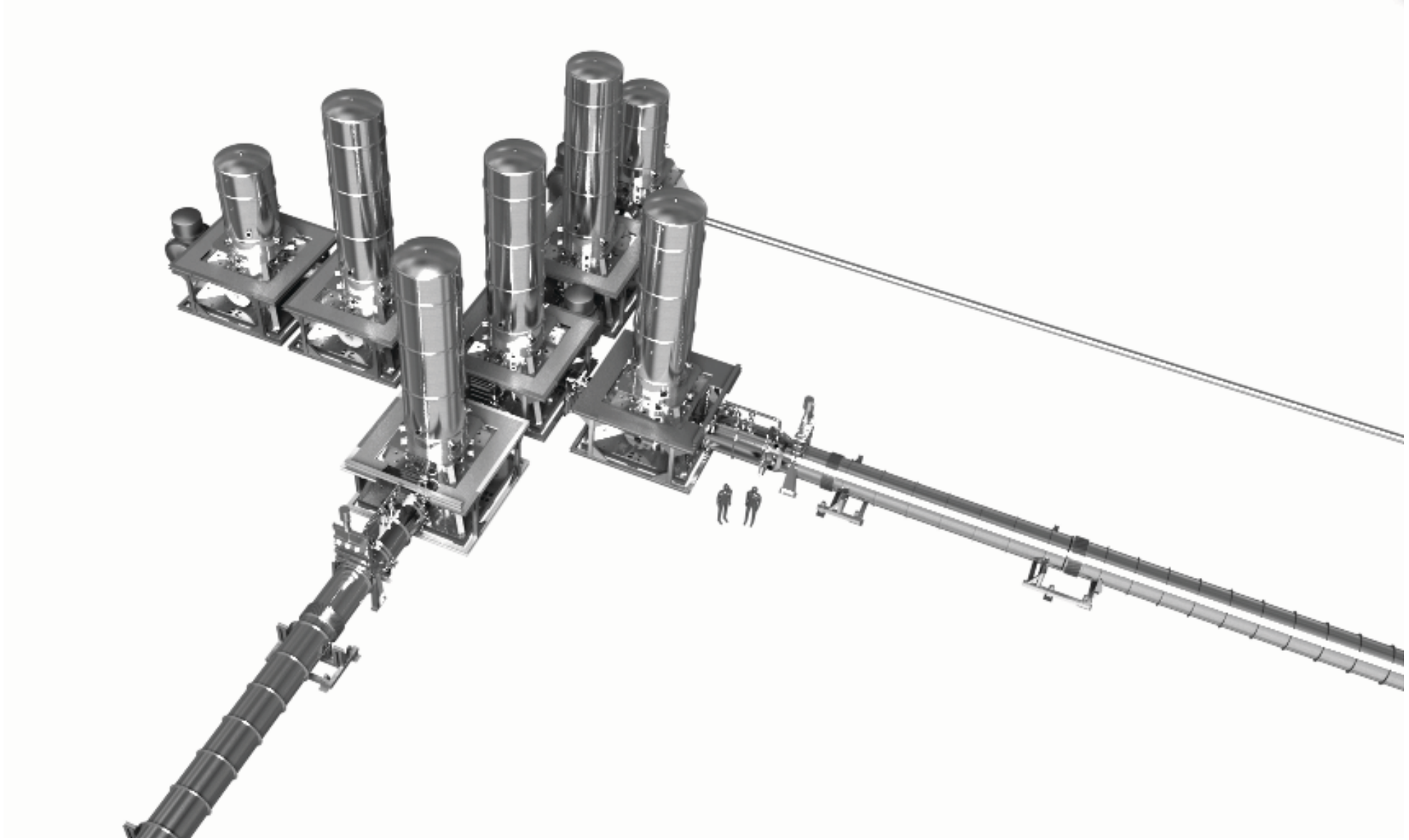

Figure 29. rendering of the vacuum chambers in the 'central area'

Five interferometer mirrors and two benches are suspended to superattenuators in the central building.

Credits: Cyril Frésillon/Virgo/Photothèque CNRS

The Advanced Virgo benches are suspended to an attenuator and placed in vacuum to isolate them from vibrations from the ground and from environmental sounds.

Credits: Cyril Frésillon/Virgo/Photothèque CNRS

The Virgo north vacuum tube, 1.2 m in diameter, inside its 3 km long tunnel.

Credit: Virgo Collaboration

The Virgo 3 km long north tunnel.


The Virgo 3 km long west tunnel.


European Gravitational Observatory (Centro...
Via Eduardo Amaldi
Via E Amaldi
Via E Amaldi
Via E Amaldi
Via E Amaldi
Via E Amaldi

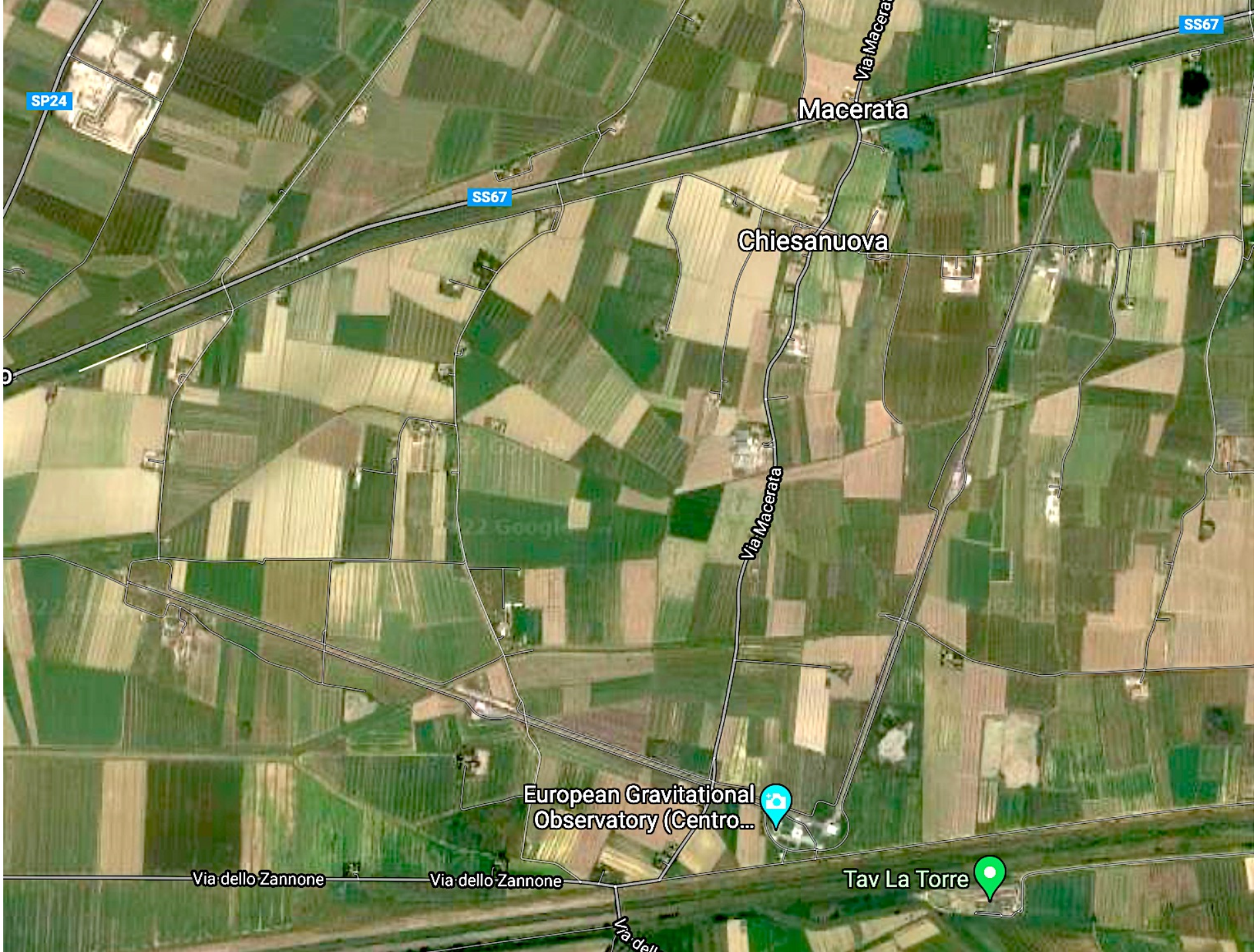
SS67
SP24
Macerata
SS67
Chiesanuova
Via Macerata
European Gravitational Observatory (Centro...
Via dello Zannone
Via dello Zannone
Tav La Torre

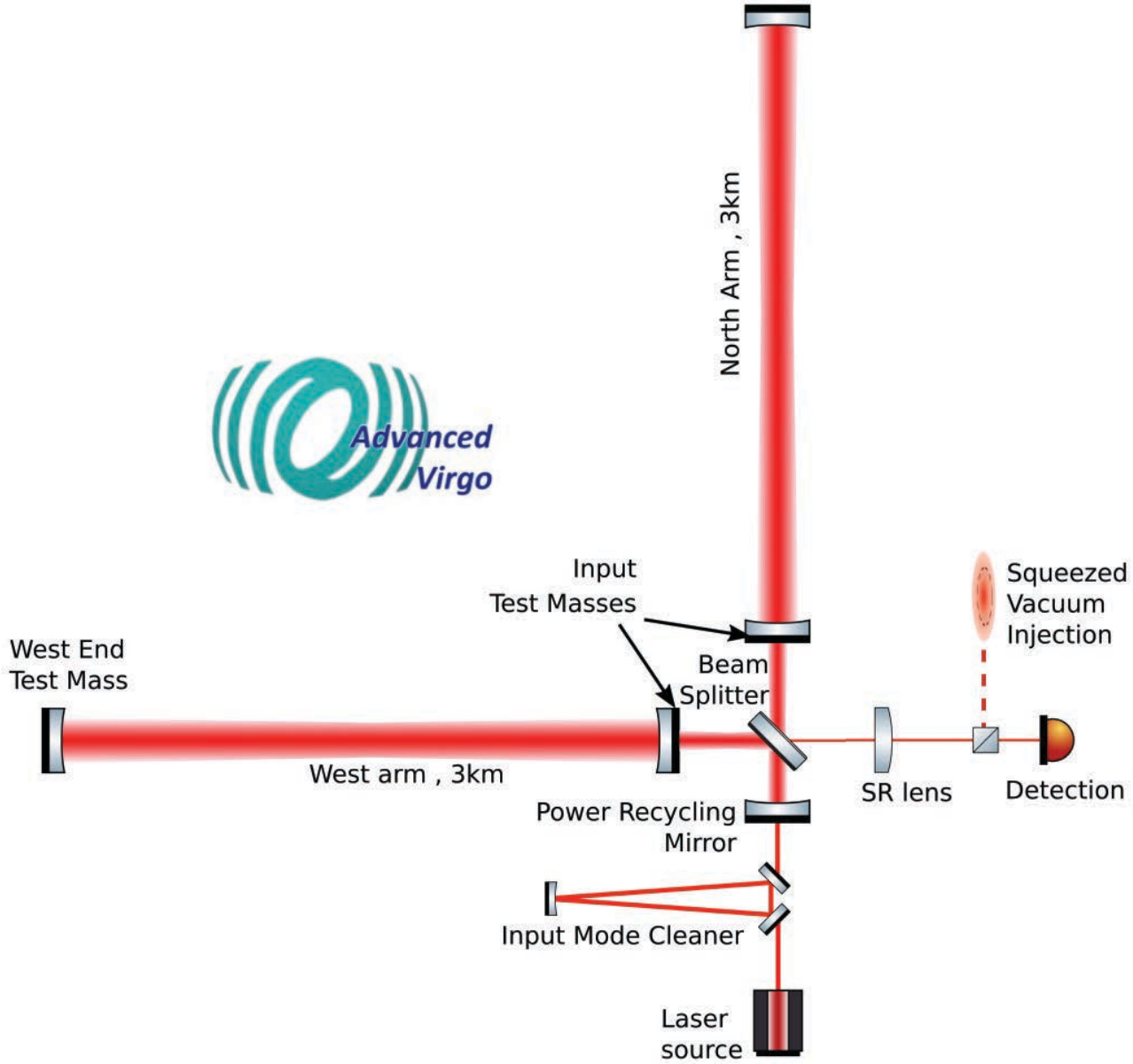

The arms of a gravitational interferometer like Virgo are more complex than a pair of end mirrors, they include *Fabry-Perot resonant cavities*.

This clearly defines the test masses and leads to a large amplitude gain.

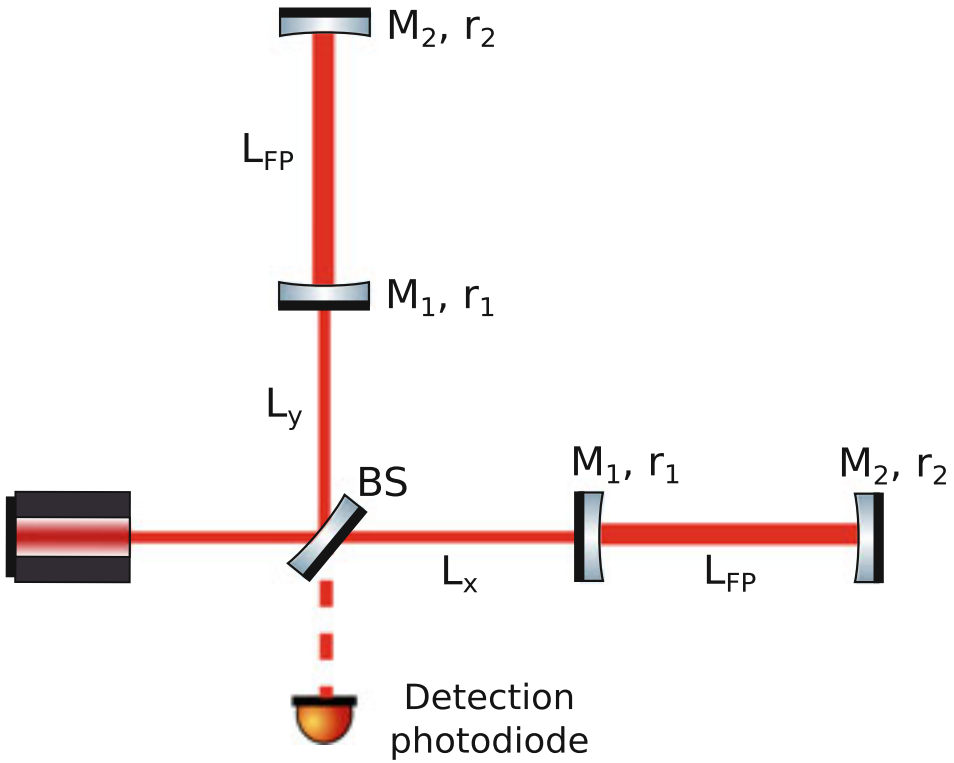

Scheme of a Michelson interferometer with Fabry-Perot cavities on its arms

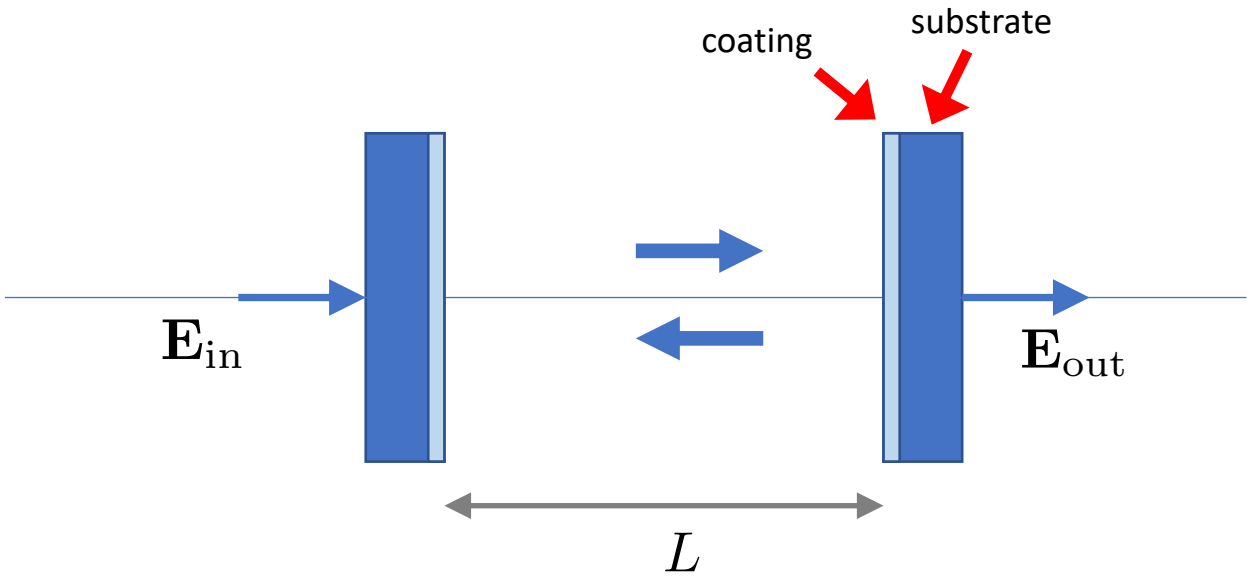

Basic scheme of a Fabry-Perot resonant cavity

Standard theory of Fabry-Perot resonant cavities: mirrors with equal (and real) reflectivity and transmission coefficients, no absorption

Energy conservation means $|\mathcal{R}|^2 + |\mathcal{T}|^2 = 1$

$$\mathbf{E}_{\text{inside}} = \mathcal{T}\mathbf{E}_{\text{in}} + \mathcal{T}\mathcal{R}^2\mathbf{E}_{\text{in}}e^{i2kL} + \mathcal{T}\mathcal{R}^4\mathbf{E}_{\text{in}}e^{i4kL} + \dots$$

$$= \mathcal{T}\mathbf{E}_{\text{in}} \sum_{n=0}^{\infty} \mathcal{R}^{2n} e^{2inkL}$$

$$= \frac{\mathcal{T}}{1 - \mathcal{R}^2 e^{2ikL}}\, \mathbf{E}_{\text{in}}$$

Here we drop the time dependence (assuming perfect coherence of light)

$$\mathbf{E}_{\text{out}} = \frac{\mathcal{T}^2}{1 - \mathcal{R}^2 e^{2ikL}}\, \mathbf{E}_{\text{in}}; \quad H(\omega) = \frac{E_{\text{out}}}{E_{\text{in}}} = \frac{\mathcal{T}^2}{1 - \mathcal{R}^2 e^{2ikL}}$$

This is the transfer function of the F-P cavity

$$\mathbf{E}_{\text{out}} = \frac{\mathcal{T}^2 e^{ikL}}{1 - \mathcal{R}^2 e^{2ikL}}\,\mathbf{E}_{\text{in}} = \frac{\mathcal{T}^2}{(1 - \mathcal{R}^2\cos 2kL) - i\mathcal{R}^2 \sin 2kL}\,\mathbf{E}_{\text{in}} e^{ikL}$$

$$= \frac{T}{(1 - R\cos 2kL) - iR\sin 2kL}\,\mathbf{E}_{\text{in}} e^{ikL}$$

Again, remember that transmittivity and reflectivity are both real here

$$P_{\text{out}} = \frac{T^2}{1 - 2R\cos 2kL + R^2}\,P_{\text{in}} = \frac{(1-R)^2}{(1-R)^2 + 2R(1-\cos 2kL)}\,P_{\text{in}}$$

$$= \frac{(1-R)^2}{(1-R)^2 + 4R\sin^2 kL}\,P_{\text{in}}$$

$$= \frac{1}{1 + 4R\sin^2 kL/(1-R)^2}\,P_{\text{in}}$$

$$= \frac{1}{1 + \left(\frac{2\mathcal{F}}{\pi}\right)^2 \sin^2 kL}\,P_{\text{in}}$$

$$\mathcal{F} = \frac{\pi\sqrt{R}}{1-R}$$

this is the ***finesse*** of the resonant cavity

Airy's function

$$\frac{1}{1+\left(\frac{2\mathcal{F}}{\pi}\right)^2 \sin^2 kL}$$

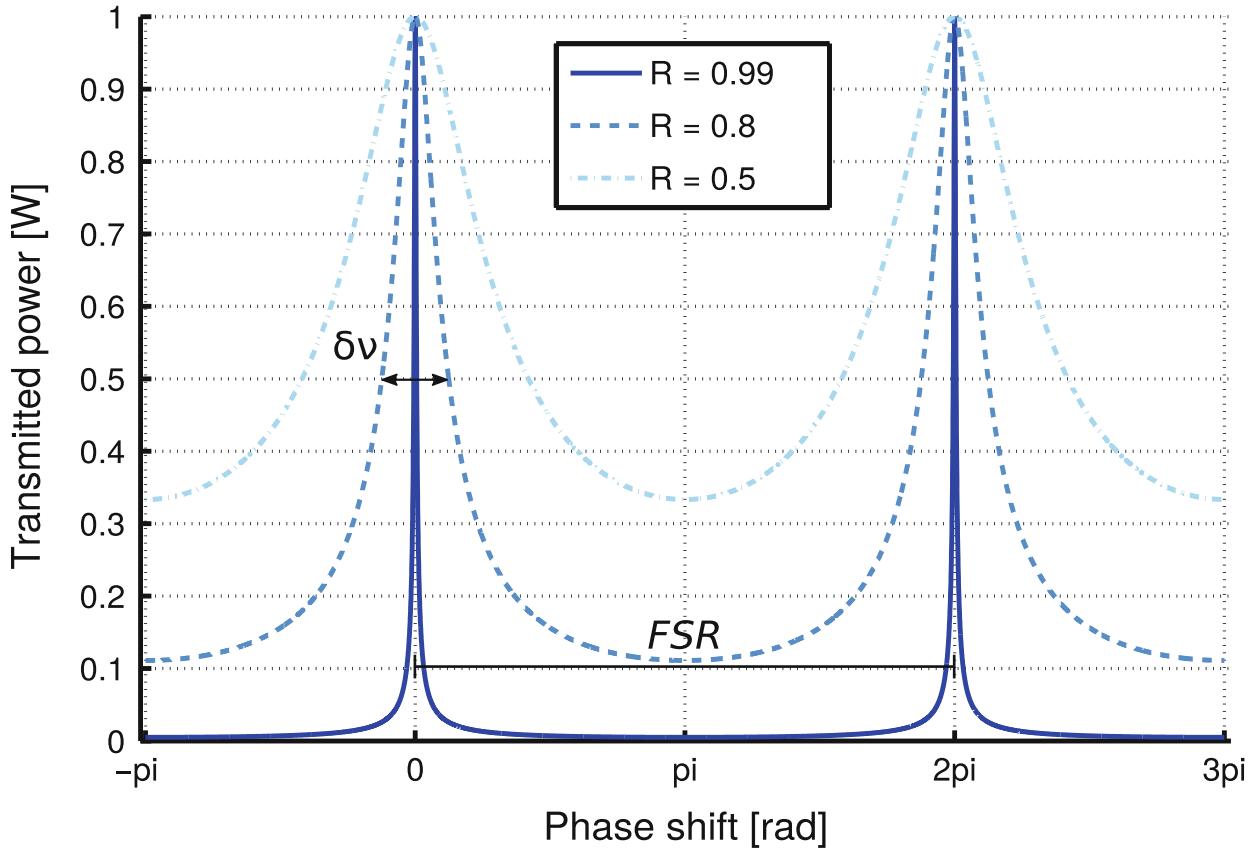

(Phase shift 2*kL* accumulated in a complete round trip)

Airy's function

$$\frac{1}{1+\left(\frac{2\mathcal{F}}{\pi}\right)^2 \sin^2 kL}$$

resonance condition $kL = n\pi$

$$\Rightarrow \nu_n = \frac{nc}{2L} \quad \Rightarrow \boxed{\mathrm{FSR} = \frac{c}{2L}}$$

(FSR = Free Spectral Range)

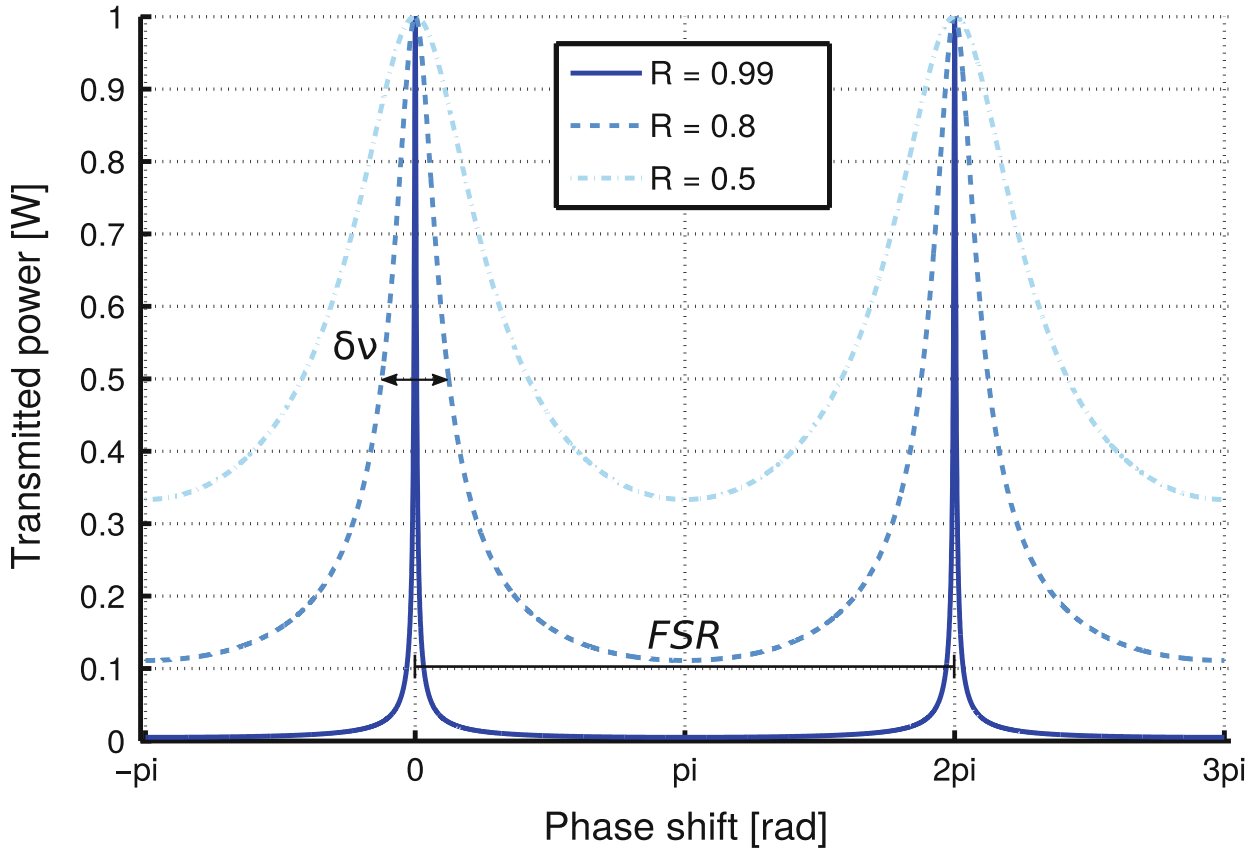

(Phase shift 2*kL* accumulated in a complete round trip)

linewidth from the solution of

$$\left(\frac{2\mathcal{F}}{\pi}\right)^2 \sin^2 kL = 1 \;\Rightarrow\; \frac{\pi}{2}\,\frac{1}{\mathcal{F}} = \sin kL \approx kL = \frac{2\pi\nu}{c}L$$

$$\boxed{\delta\nu = \frac{c}{2L}\,\frac{1}{\mathcal{F}} = \frac{\mathrm{FSR}}{\mathcal{F}}}$$

first peak at nonzero frequency (FSR)

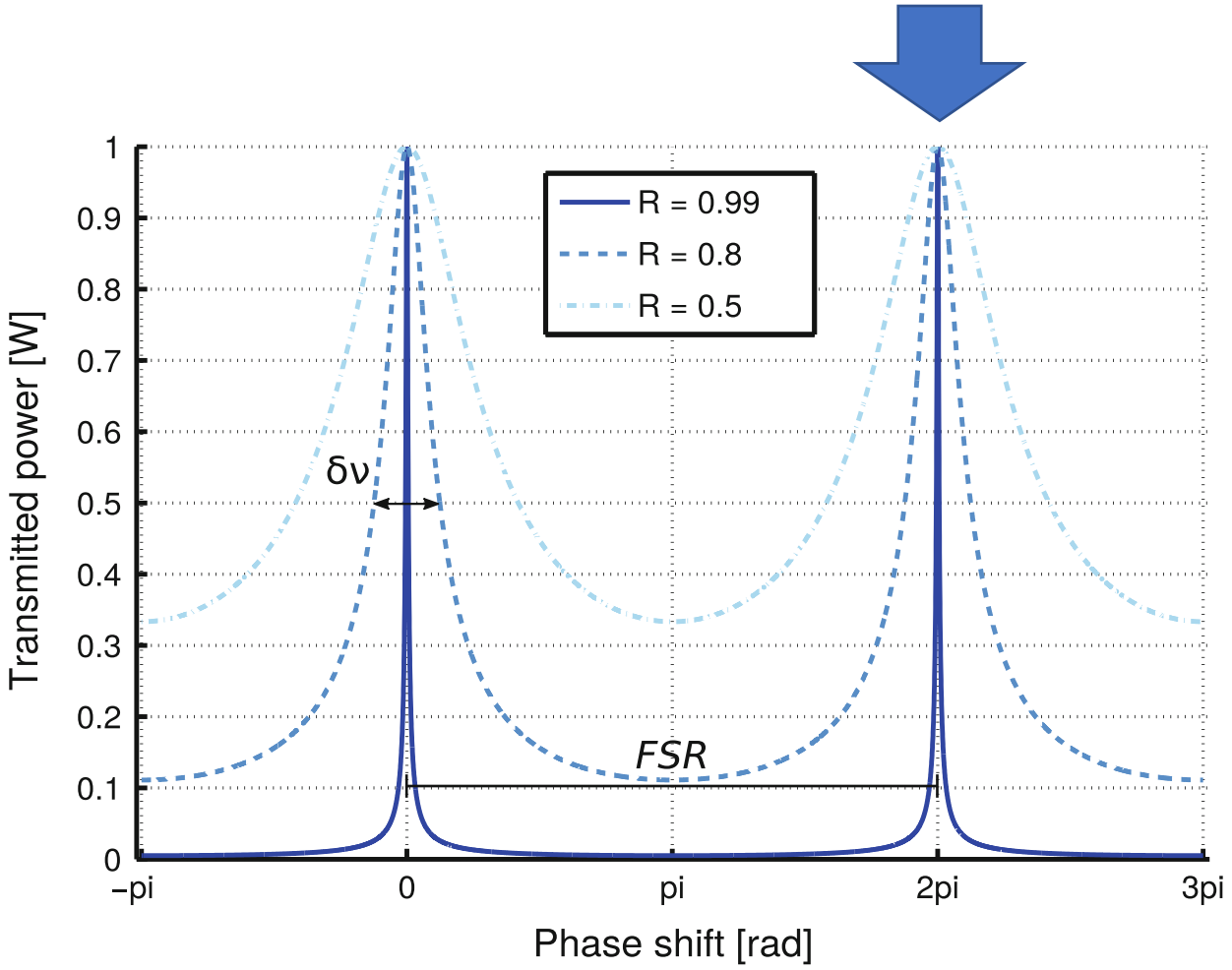

Analogy with the harmonic oscillator

$$Q = \frac{\omega_0}{\Gamma} \quad \rightarrow \quad \mathcal{F} = \frac{\mathrm{FSR}}{\delta\nu}$$

"**photon lifetime**" inside the resonant cavity (on resonance)

$$\tau = \frac{1}{\Gamma} \quad \rightarrow \quad \tau = \frac{1}{2\pi\delta\nu}$$

or also

$$\tau = \frac{\mathcal{F}}{2\pi\ \mathrm{FSR}}; \quad n = \frac{c\tau}{2L} = \mathrm{FSR}\ \tau = \frac{\mathcal{F}}{2\pi}$$

average number of back-and-forth passes inside cavity

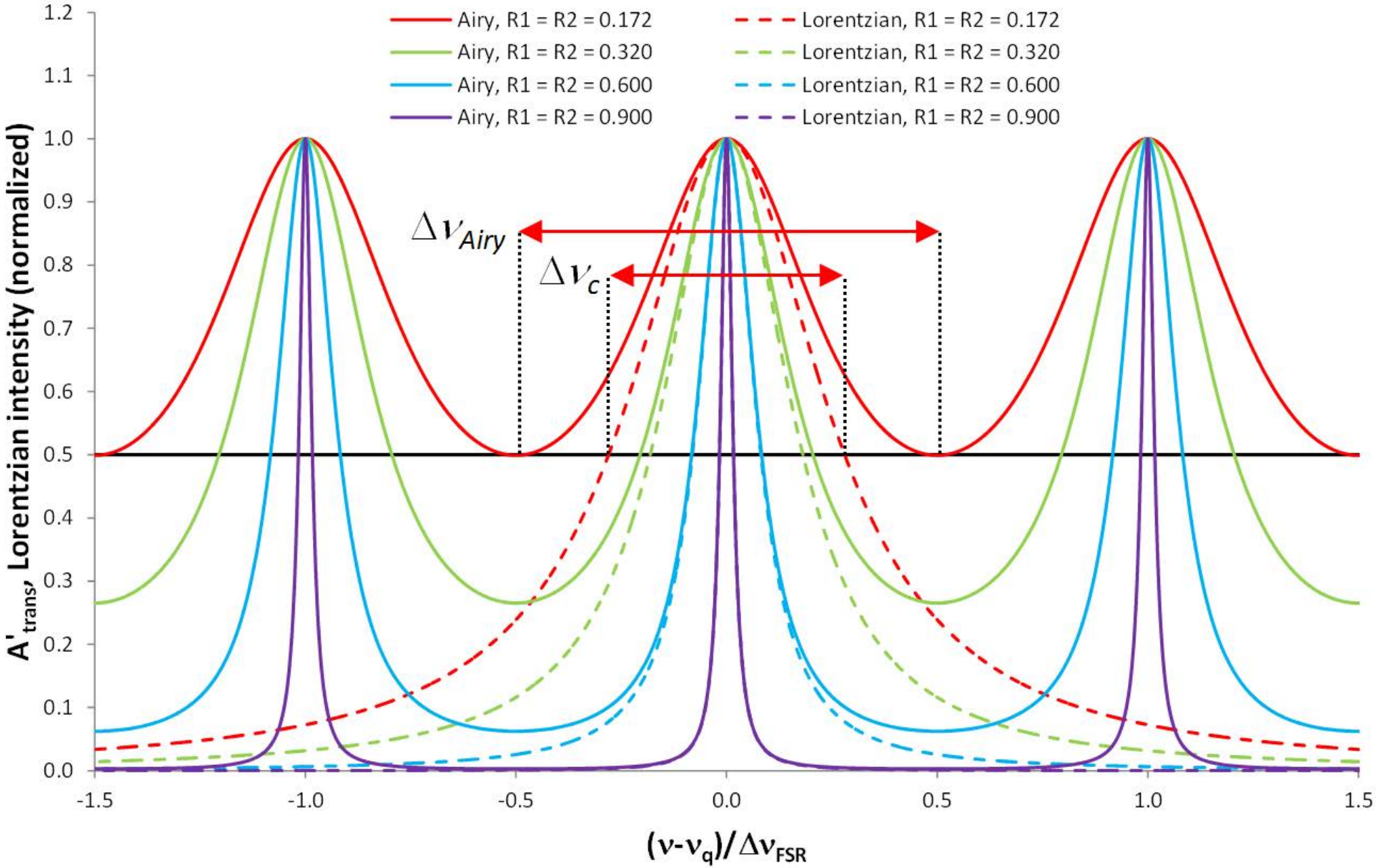
Airy, R1 = R2 = 0.172
Airy, R1 = R2 = 0.320
Airy, R1 = R2 = 0.600
Airy, R1 = R2 = 0.900
Lorentzian, R1 = R2 = 0.172
Lorentzian, R1 = R2 = 0.320
Lorentzian, R1 = R2 = 0.600
Lorentzian, R1 = R2 = 0.900
$\Delta\nu_{Airy}$
$\Delta\nu_c$
A'trans, Lorentzian intensity (normalized)
(ν-νq)/ΔνFSR
1.2
1.1
1.0
0.9
0.8
0.7
0.6
0.5
0.4
0.3
0.2
0.1
0.0
-1.5
-1.0
-0.5
0.0
0.5
1.0
1.5

Ray confinement in a Fabry-Perot resonant cavity

(simple geometrical optics approach)

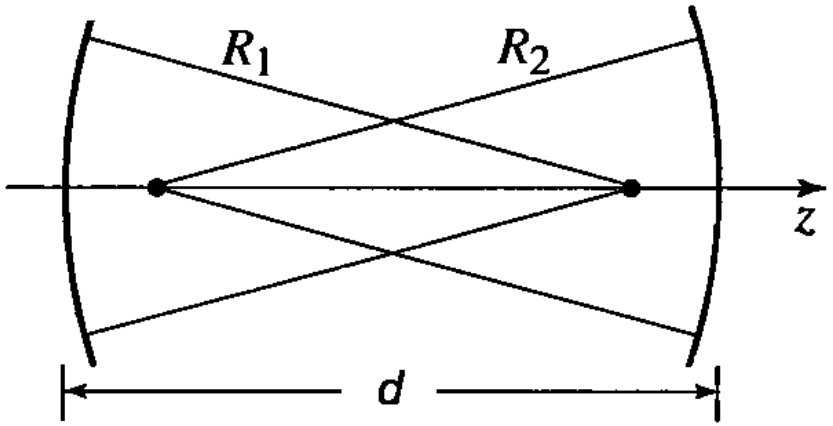

Geometry of a spherical-mirror resonator. In this illustration both mirrors are concave (their radii of curvature are negative).

Methodological aside: matrix optics

(from Saleh&Teich, *Fundamentals of Photonics*, 2nd ed. Wiley 2007; for a concise explanation, see also https://www.rp-photonics.com/abcd_matrix.html)

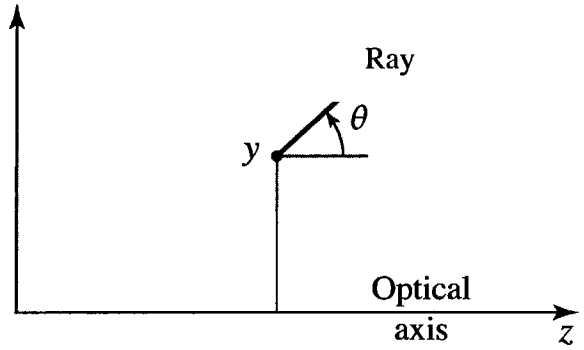

Figure 1.4-1 A ray is characterized by its coordinate y and its angle θ.

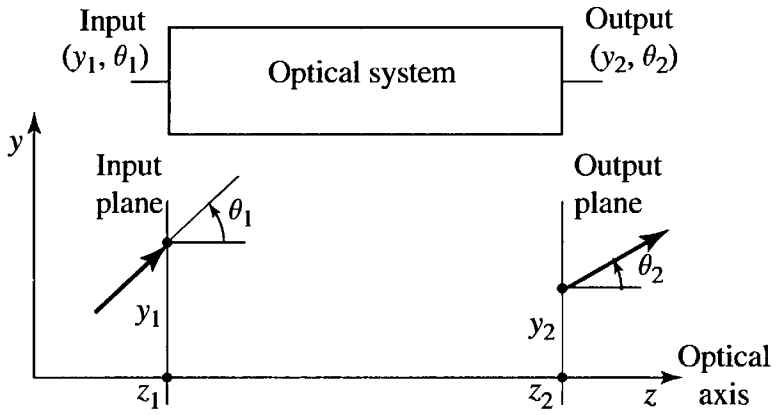

Figure 1.4-2 A ray enters an optical system at location z_1 with position y_1 and angle θ_1 and leaves at position y_2 and angle θ_2.

In the paraxial approximation (small angles, so that $\sin x \approx x$)

$$y_2 = Ay_1 + B\theta_1$$
$$\theta_2 = Cy_1 + D\theta_1$$

$$\begin{pmatrix} y_2 \\ \theta_2 \end{pmatrix} = \begin{pmatrix} A & B \\ C & D \end{pmatrix} \begin{pmatrix} y_1 \\ \theta_1 \end{pmatrix}$$

Effect of optical element encoded in this matrix (ray transfer matrix)

Free-Space Propagation

Since rays travel along straight lines in a medium of uniform refractive index such as free space, a ray traversing a distance d is altered in accordance with $y_2 = y_1 + \theta_1 d$ and $\theta_2 = \theta_1$. The ray-transfer matrix is therefore

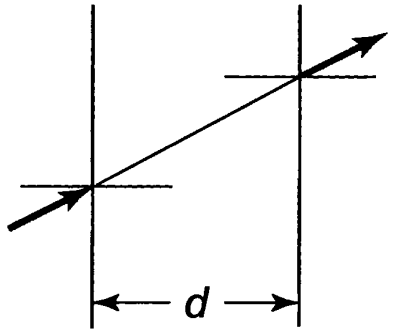

$$\mathbf{M} = \begin{bmatrix} 1 & d \\ 0 & 1 \end{bmatrix}. \qquad (1.4\text{-}4)$$

Refraction at a Planar Boundary

At a planar boundary between two media of refractive indexes n_1 and n_2, the ray angle changes in accordance with Snell's law $n_1 \sin\theta_1 = n_2 \sin\theta_2$. In the paraxial approximation, $n_1\theta_1 \approx n_2\theta_2$. The position of the ray is not altered, $y_2 = y_1$. The ray-transfer matrix is

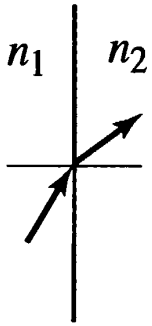

$$\mathbf{M} = \begin{bmatrix} 1 & 0 \\ 0 & \frac{n_1}{n_2} \end{bmatrix}. \qquad (1.4\text{-}5)$$

Refraction at a spherical boundary

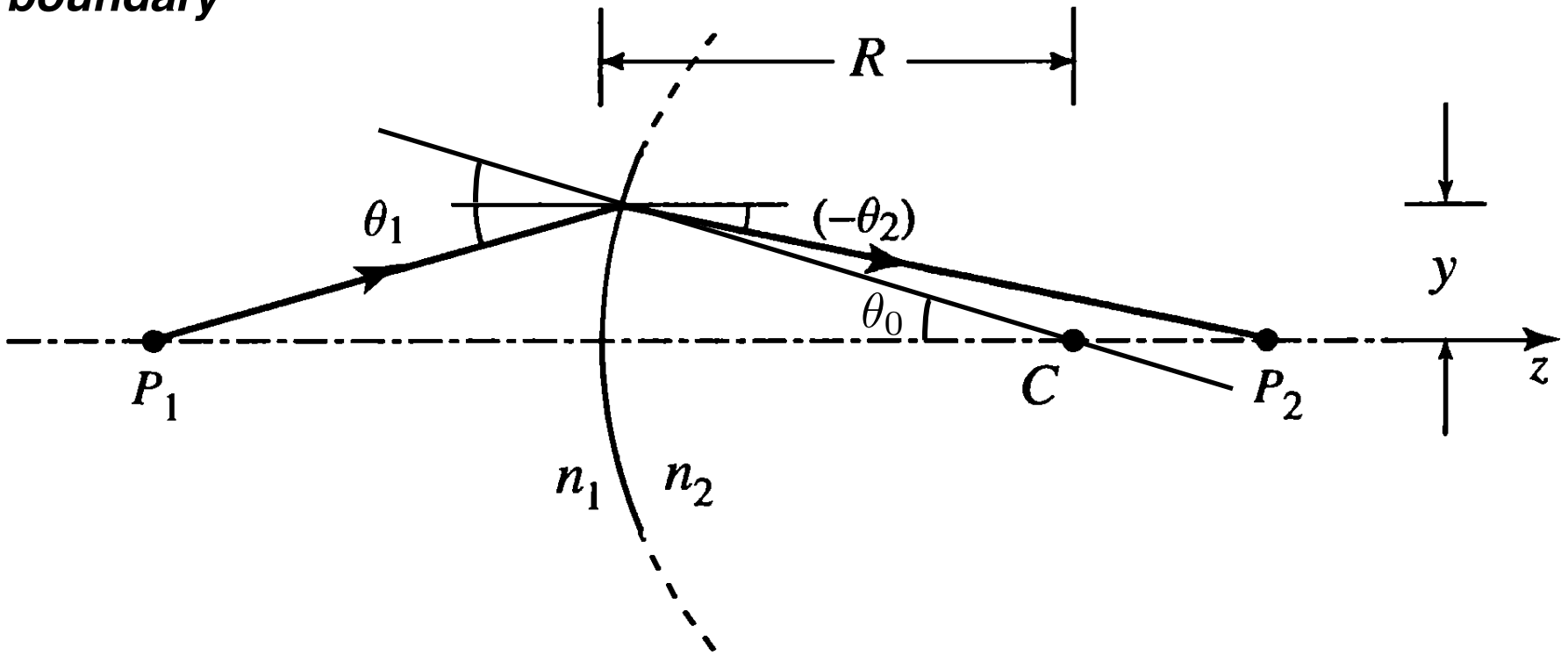

$$n_1(\theta_1 + \theta_0) = n_2\left[\theta_0 - (-\theta_2)\right]$$

$$\theta_0 \approx y/R$$

$$\Rightarrow \quad \theta_2 = -\frac{n_2 - n_1}{n_2 R} y + \frac{n_1}{n_2}\theta_1$$

Refraction at a Spherical Boundary

The relation between θ_1 and θ_2 for paraxial rays refracted at a spherical boundary between two media is provided in (1.2-8). The ray height is not altered, $y_2 \approx y_1$. The ray-transfer matrix is

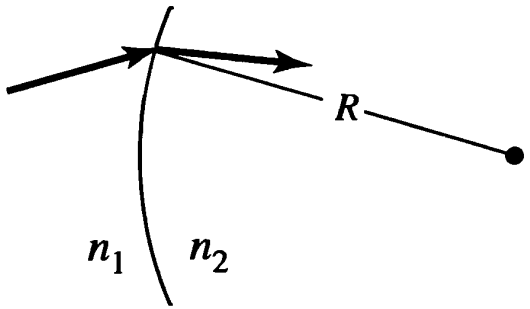

Convex: $R > 0$; concave: $R < 0$

$$\mathbf{M} = \begin{bmatrix} 1 & 0 \\ -\frac{(n_2 - n_1)}{n_2 R} & \frac{n_1}{n_2} \end{bmatrix}. \qquad (1.4\text{-}6)$$

Transmission Through a Thin Lens

The relation between θ_1 and θ_2 for paraxial rays transmitted through a thin lens of focal length f is given in (1.2-11). Since the height remains unchanged $(y_2 = y_1)$, we have

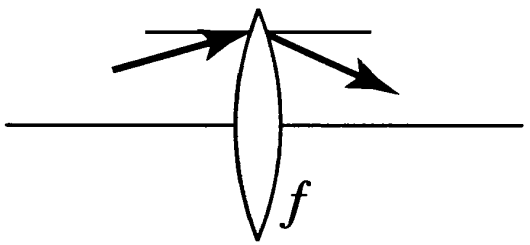

Convex: $f > 0$; concave: $f < 0$

$$\mathbf{M} = \begin{bmatrix} 1 & 0 \\ -\frac{1}{f} & 1 \end{bmatrix}. \qquad (1.4\text{-}7)$$

prove this result!

Reflection from a Planar Mirror

Upon reflection from a planar mirror, the ray position is not altered, $y_2 = y_1$. Adopting the convention that the z axis points in the general direction of travel of the rays, i.e., toward the mirror for the incident rays and away from it for the reflected rays, we conclude that $\theta_2 = \theta_1$. The ray-transfer matrix is therefore the identity matrix

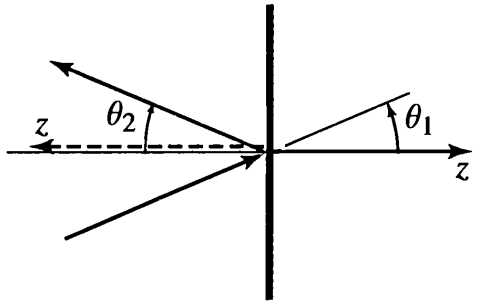

$$\mathbf{M} = \begin{bmatrix} 1 & 0 \\ 0 & 1 \end{bmatrix}. \qquad (1.4\text{-}8)$$

Reflection from a Spherical Mirror

Using (1.2-1), and the convention that the z axis follows the general direction of the rays as they reflect from mirrors, we similarly obtain

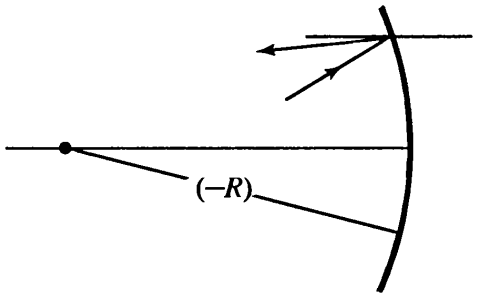

Concave: $R < 0$; convex: $R > 0$

$$\mathbf{M} = \begin{bmatrix} 1 & 0 \\ \frac{2}{R} & 1 \end{bmatrix}. \qquad (1.4\text{-}9)$$

prove this result!

Note the similarity between the ray-transfer matrices of a spherical mirror (1.4-9) and a thin lens (1.4-7). A mirror with radius of curvature R bends rays in a manner that is identical to that of a thin lens with focal length $f = -R/2$.

Important remark:

in all cases considered here, the determinant of the ray transfer matrix is

$$\det \mathbf{M} = \frac{n_1}{n_2} \quad \rightarrow \quad 1$$

homogenous environment (same refractive index) or vacuum

C. Matrices of Cascaded Optical Components

A cascade of N optical components or systems whose ray-transfer matrices are $\mathbf{M}_1, \mathbf{M}_2, \ldots, \mathbf{M}_N$ is equivalent to a single optical system of ray-transfer matrix

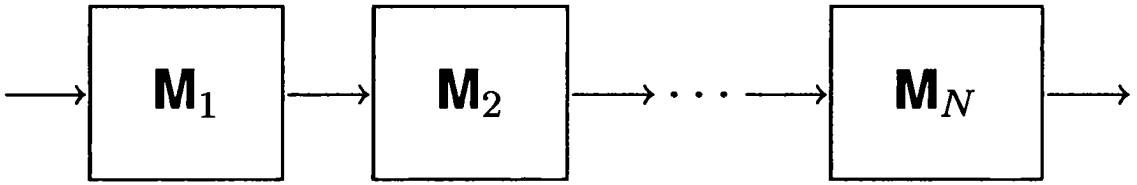

$$\mathbf{M} = \mathbf{M}_N \cdots \mathbf{M}_2 \mathbf{M}_1. \tag{1.4-10}$$

Note the order of matrix multiplication: The matrix of the system that is crossed by the rays is first placed to the right, so that it operates on the column matrix of the incident ray first. A sequence of matrix multiplications is not, in general, commutative, although it is associative.

EXERCISE 1.4-3

A Gap Followed by a Thin Lens. Show that the ray-transfer matrix of a distance d of free space followed by a lens of focal length f is

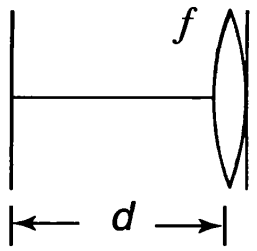

$$\mathbf{M} = \begin{bmatrix} 1 & d \\ -\frac{1}{f} & 1 - \frac{d}{f} \end{bmatrix}. \qquad (1.4\text{-}12)$$

EXERCISE 1.4-4

Imaging with a Thin Lens. Derive an expression for the ray-transfer matrix of a system comprised of free space/thin lens/free space, as shown in Fig. 1.4-3. Show that if the imaging condition $(1/d_1 + 1/d_2 = 1/f)$ is satisfied, all rays originating from a single point in the input plane reach the output plane at the single point y_2, regardless of their angles. Also show that if $d_2 = f$, all parallel incident rays are focused by the lens onto a single point in the output plane.

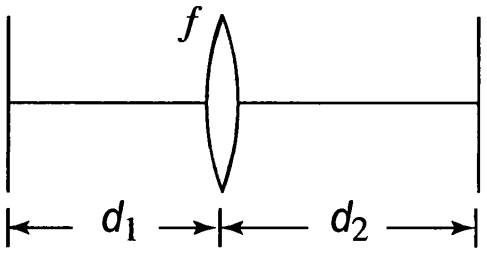

Figure 1.4-3 Single-lens imaging system.

Propagation in periodic systems

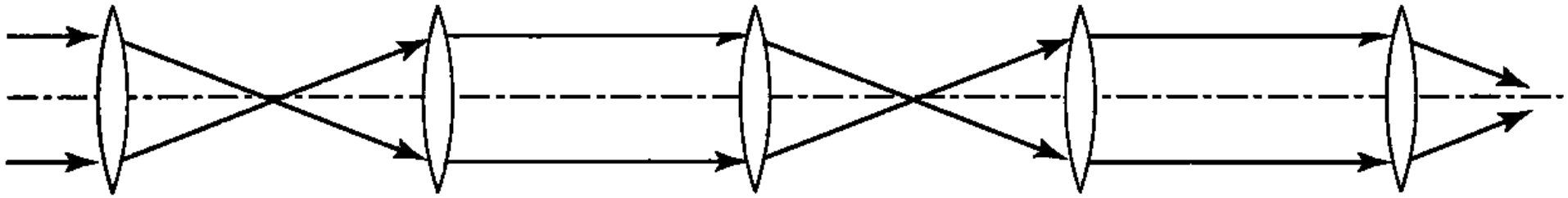

Example of periodic optical system

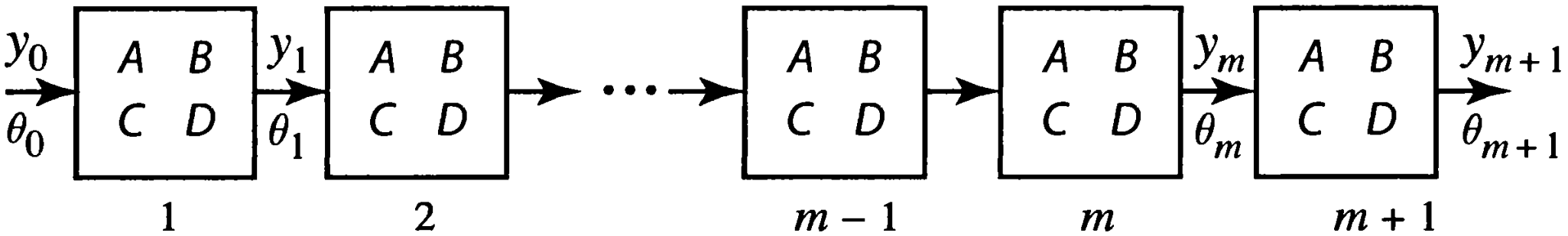

A periodic optical system can be studied by repeatedly applying the same ray transfer matrix

To determine the position and slope (y_m, θ_m) of the ray at the exit of the mth stage, we apply the $ABCD$ matrix m times,

$$\begin{bmatrix} y_m \\ \theta_m \end{bmatrix} = \begin{bmatrix} A & B \\ C & D \end{bmatrix}^m \begin{bmatrix} y_0 \\ \theta_0 \end{bmatrix}. \tag{1.4-18}$$

We can also iteratively apply the relations

$$y_{m+1} = Ay_m + B\theta_m \tag{1.4-19}$$

$$\theta_{m+1} = Cy_m + D\theta_m \tag{1.4-20}$$

It is of interest to derive equations that govern the dynamics of the position y_m, $m = 0, 1, \ldots$, irrespective of the angle θ_m. This is achieved by eliminating θ_m from (1.4-19) and (1.4-20).

$$y_{m+1} = Ay_m + B\theta_m \tag{1.4-19}$$

$$\theta_{m+1} = Cy_m + D\theta_m \tag{1.4-20}$$

$$\theta_m = \frac{y_{m+1} - Ay_m}{B}. \tag{1.4-21}$$

Replacing m with $m + 1$ in (1.4-21) yields

$$\theta_{m+1} = \frac{y_{m+2} - Ay_{m+1}}{B}. \tag{1.4-22}$$

Substituting (1.4-21) and (1.4-22) into (1.4-20) gives

$$\boxed{y_{m+2} = 2by_{m+1} - F^2 y_m,} \tag{1.4-23}$$

Recurrence Relation for Ray Position

$$\theta_m = \frac{y_{m+1} - Ay_m}{B}. \tag{1.4-21}$$

Replacing m with $m + 1$ in (1.4-21) yields

$$\theta_{m+1} = \frac{y_{m+2} - Ay_{m+1}}{B}. \tag{1.4-22}$$

Substituting (1.4-21) and (1.4-22) into (1.4-20) gives

$$\boxed{y_{m+2} = 2by_{m+1} - F^2 y_m,} \tag{1.4-23}$$

Recurrence Relation for Ray Position

where

$$b = \frac{A + D}{2} \tag{1.4-24}$$

$$F^2 = AD - BC = \det[\mathbf{M}], \tag{1.4-25}$$

An approach based on the formalism of generating functions, suggests a solution of the following form (prove it if you know this formalism)

$$y_m = y_0 h^m \tag{1.4-26}$$

where h is a constant. Substituting (1.4-26) into (1.4-23) immediately shows that the trial solution is suitable provided that h satisfies the quadratic algebraic equation

$$h^2 - 2bh + F^2 = 0, \tag{1.4-27}$$

from which

$$h = b \pm j\sqrt{F^2 - b^2}. \tag{1.4-28}$$

The results can be presented in a more compact form by defining the variable

$$\varphi = \cos^{-1}(b/F), \tag{1.4-29}$$

$$\varphi = \arccos(b/F) \quad \Rightarrow \quad b = F\cos\varphi; \quad \sqrt{F^2 - b^2} = F\sin\varphi$$

$$\Rightarrow \quad h = F(\cos\varphi + i\sin\varphi) = Fe^{i\varphi}$$

$$\Rightarrow \quad y_m = y_0 F^m e^{im\varphi}$$

A general solution may be constructed from the two solutions with positive and negative signs by forming their linear combination. The sum of the two exponential functions can always be written as a harmonic (circular) function, so that

$$y_m = y_{\max} F^m \sin(m\varphi + \varphi_0), \tag{1.4-30}$$

where $y_{\max}$ and φ_0 are constants to be determined from the initial conditions y_0 and y_1. In particular, setting $m = 0$ we obtain $y_{\max} = y_0/\sin\varphi_0$.

In the case of mirrors, the determinant

$$\det \mathbf{M} = 1$$

therefore

$$F = \sqrt{\det \mathbf{M}} = 1$$

and the solution is

$$\boxed{y_m = y_{\max} \sin(m\varphi + \varphi_0).}$$

(1.4-31)
Ray Position
Periodic System

Ray confinement in a Fabry-Perot resonant cavity

(simple geometrical optics approach)

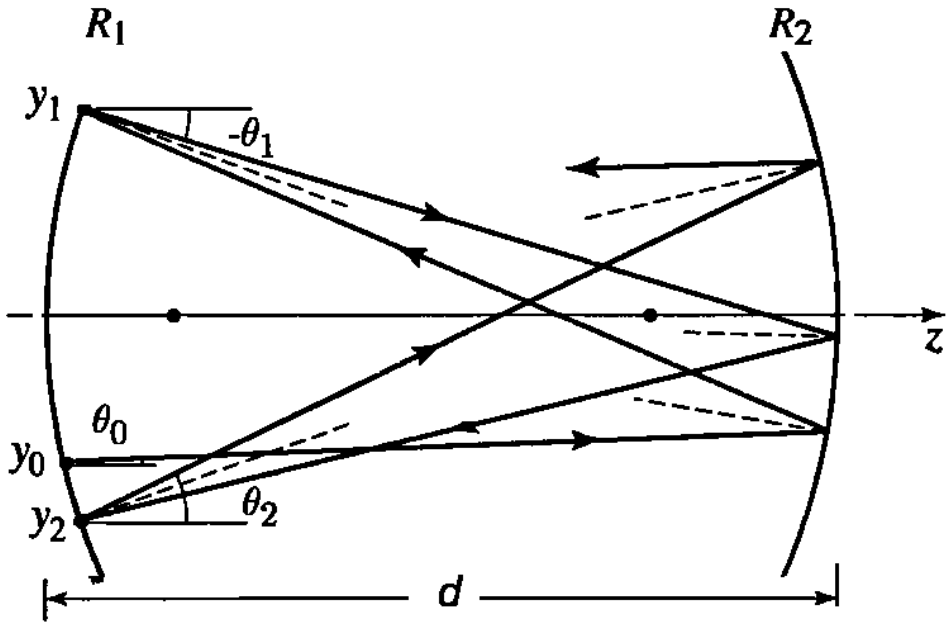

Figure 10.2-2 The position and inclination of a ray after m round trips are represented by y_m and θ_m, respectively, where $m = 0, 1, 2, \ldots$. In this diagram, $\theta_1 < 0$ since the ray is directed downward. Angles are exaggerated for the purposes of illustration; all rays are paraxial so that $\sin\theta \approx \tan\theta \approx \theta$ and the propagation distance of all rays between the mirrors is $\approx d$.

In this discussion, we limit ourselves to

- paraxial rays
- meridional rays (rays that lie in a plane through the optical axis)

The system is periodic, with round-trip transfer matrix

$$\begin{bmatrix} A & B \\ C & D \end{bmatrix} = \begin{bmatrix} 1 & 0 \\ \frac{2}{R_1} & 1 \end{bmatrix} \begin{bmatrix} 1 & d \\ 0 & 1 \end{bmatrix} \begin{bmatrix} 1 & 0 \\ \frac{2}{R_2} & 1 \end{bmatrix} \begin{bmatrix} 1 & d \\ 0 & 1 \end{bmatrix}. \qquad (10.2\text{-}2)$$

i.e.,

- Propagation a distance d through free space
- Reflection from a mirror of radius R_2
- Propagation a distance d through free space
- Reflection from a mirror of radius R_1

For the case at hand $F = 1$, so that

$$y_m = y_{\max} \sin(m\varphi + \varphi_0), \tag{10.2-3}$$

$$\varphi = \cos^{-1} b, \qquad b = 2\left(1 + \frac{d}{R_1}\right)\left(1 + \frac{d}{R_2}\right) - 1. \tag{10.2-4}$$

The solution (10.2-3) is harmonic, and therefore bounded, provided $\varphi = \cos^{-1} b$ is real. This is ensured if $|b| \leq 1$, i.e., if $-1 \leq b \leq 1$, so that

$$0 \leq \left(1 + \frac{d}{R_1}\right)\left(1 + \frac{d}{R_2}\right) \leq 1. \tag{10.2-5}$$

It is convenient to write this condition in terms of the quantities $g_1 = 1 + d/R_1$ and $g_2 = 1 + d/R_2$, which are known as the ***g* parameters**:

$$\boxed{0 \leq g_1\, g_2 \leq 1.} \tag{10.2-6}$$

Confinement Condition

$$0 \leq g_1 g_2 \leq 1. \qquad (10.2\text{-}6)$$

Confinement Condition

The resonator is said to be **stable** when this condition is satisfied.

When the confinement condition (10.2-6) is not satisfied, φ is imaginary so that y_m in (10.2-3) becomes a hyperbolic sine function of m that increases without bound. The resonator is then said to be **unstable**. At the boundary of the confinement condition (when the inequalities are equalities), the resonator is said to be **conditionally stable**.

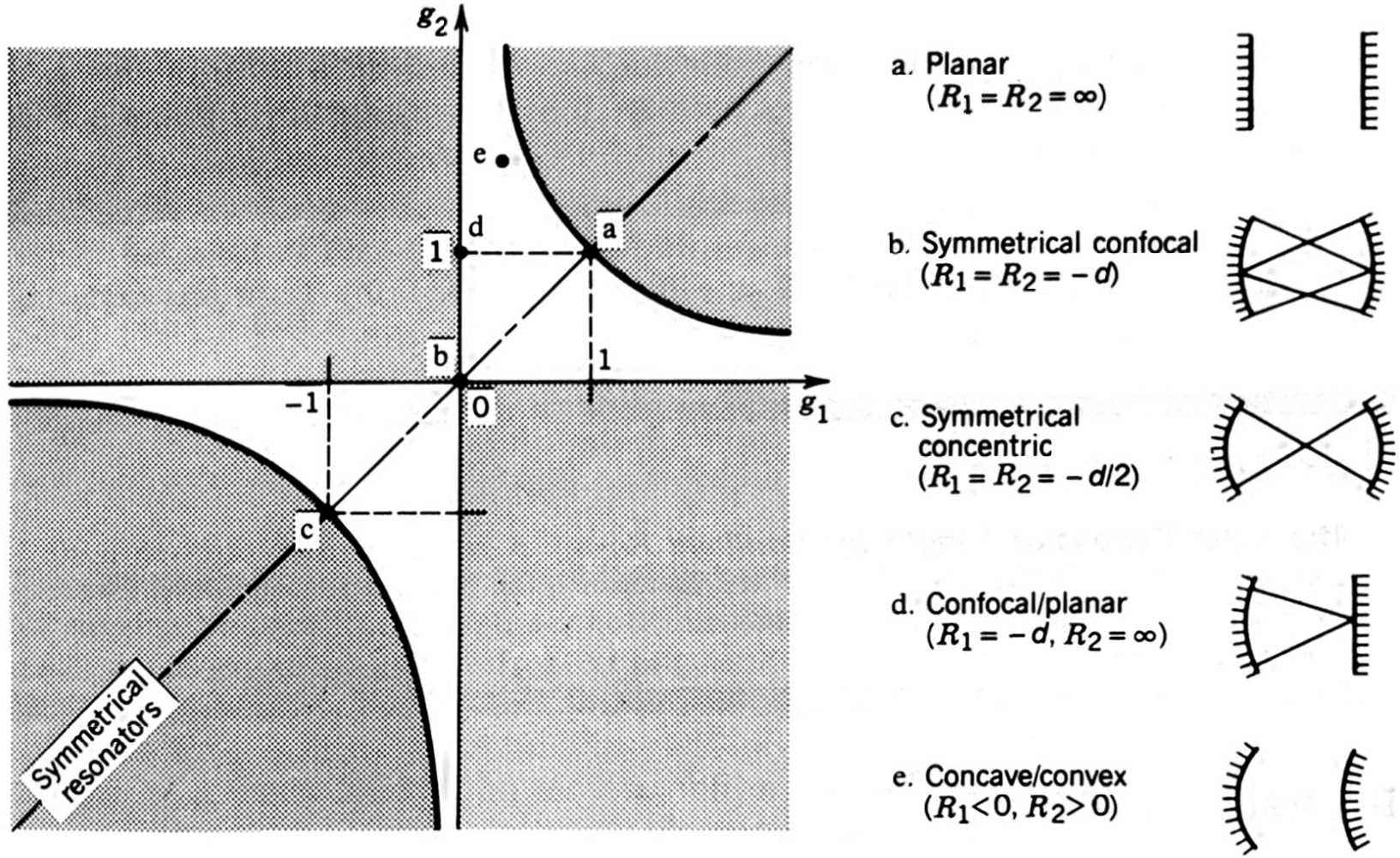

Figure 9.2-3 Resonator stability diagram. A spherical-mirror resonator is stable if the parameters $g_1 = 1 + d/R_1$ and $g_2 = 1 + d/R_2$ lie in the unshaded regions bounded by the lines $g_1 = 0$ and $g_2 = 0$, and the hyperbola $g_2 = 1/g_1$. R is negative for a concave mirror and positive for a convex mirror. Various special configurations are indicated by letters. All symmetrical resonators lie along the line $g_2 = g_1$.

Fabry-Perot resonant cavity with unequal mirrors

It is easy to see that for an FP cavity with unequal mirrors:

- intracavity field $$E_{\mathrm{inside}} = \frac{t_i}{1 - r_i r_e e^{ik2L}} E_{\mathrm{in}}$$
- reflected field $$E_{\mathrm{reflected}} = \frac{-r_i + r_e(r_i^2 + t_i^2)e^{ik2L}}{1 - r_i r_e e^{ik2L}} E_{\mathrm{in}}$$
- transmitted field $$E_{\mathrm{transmitted}} = \frac{t_i t_e e^{ikL}}{1 - r_i r_e e^{ik2L}} E_{\mathrm{in}}$$
- finesse: $$\mathcal{F} = \frac{\pi\sqrt{r_i r_e}}{1 - r_i r_e}$$

In Advanced Virgo

$$r_i = 0.993; \quad r_e = 0.999998$$

$$\Rightarrow \quad \mathcal{F} \approx 450$$

(i = input mirror; e = end mirror)

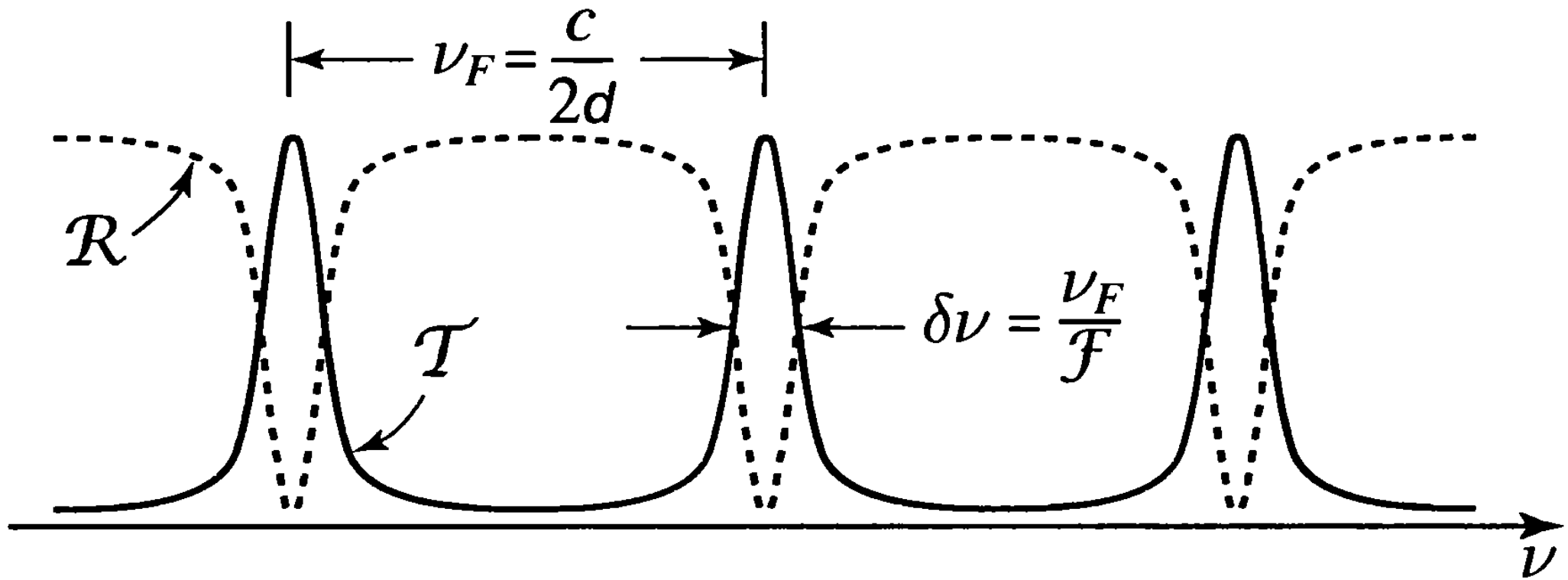

Intensity transmittance and reflectance of a Fabry-Perot resonant cavity.

Now, consider the complex (amplitude) reflection coefficient of the FP cavity

$$F = \frac{-r_i + r_e(r_i^2 + t_i^2)e^{ik2L}}{1 - r_i r_e e^{ik2L}}$$

By decomposing F in real and imaginary parts, we see that this equation represents the coordinates of a plane curve, expressed here in parametric form.

Letting $F = x + iy$ we rewrite the same equation in the form

$$F + r_i = \left[F r_i r_e + r_e(r_i^2 + t_i^2)\right] e^{ik2L}$$

$$\Rightarrow \quad |F + r_i|^2 = \left|F r_i r_e + r_e(r_i^2 + t_i^2)\right|^2$$

$$\Rightarrow \quad x^2(1 - r_i^2 r_e^2) + y^2(1 - r_i^2 r_e^2) - 2r_i\left(1 - r_e^2(r_i^2 + t_i^2)\right)x = r_e^2(r_i^2 + t_i^2)^2 - r_i^2$$

$$\Rightarrow \quad x^2 + y^2 + \frac{2r_i\left(1 - r_e^2(r_i^2 + t_i^2)\right)}{1 - r_i^2 r_e^2}x = \frac{r_e^2(r_i^2 + t_i^2)^2 - r_i^2}{1 - r_i^2 r_e^2}$$

$$\Rightarrow \quad \left[x + \frac{r_i\left(1 - r_e^2(r_i^2 + t_i^2)\right)}{1 - r_i^2 r_e^2}\right]^2 + y^2 = \frac{r_i^2\left(1 - r_e^2(r_i^2 + t_i^2)\right)^2}{(1 - r_i^2 r_e^2)^2} + \frac{r_e^2(r_i^2 + t_i^2)^2 - r_i^2}{1 - r_i^2 r_e^2}$$

The r.h.s. can be simplified further, and we obtain (prove it!):

$$\left[x + \frac{r_i\left(1 - r_e^2(r_i^2 + t_i^2)\right)}{1 - r_i^2 r_e^2}\right]^2 + y^2 = \frac{r_e^2 t_i^4}{(1 - r_i^2 r_e^2)^2}$$

which is the equation of a circle with center

$$\left\{-\frac{r_i\left[1 - r_e^2(r_i^2 + t_i^2)\right]}{1 - r_i^2 r_e^2}, 0\right\}$$

and radius

$$R = \frac{r_e t_i^2}{1 - r_i^2 r_e^2}$$

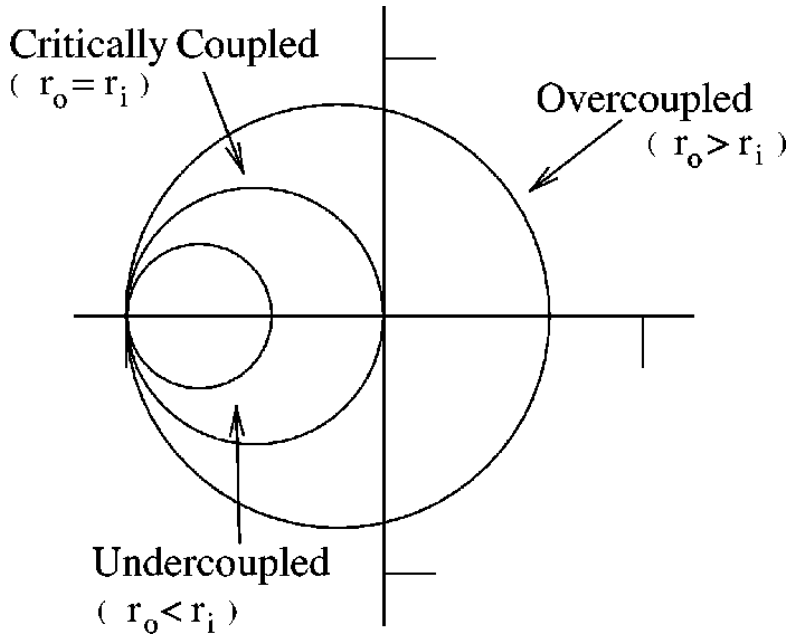

Fig. 11. The amplitude reflection coefficients for Fabry–Perot cavities are circles in the complex plane; r_i and r_o are the amplitude reflection coefficients of the input and output mirrors, respectively.

- $r_i = r_e$, critical coupling
  At resonance the reflected beam vanishes, all the incident power is transmitted through the cavity.

- $r_i < r_e$, overcoupling
  The leakage beam that bounces back from the cavity has larger amplitude than the promptly reflected beam, and there is reflection even at resonance, with positive amplitude reflection coefficient.

- $r_i > r_e$, undercoupling
  The leakage beam has a smaller amplitude than the promptly reflected beam and there is reflection even at resonance, with negative amplitude reflection coefficient.

Normally, GW interferometers are operated with overcoupled FP cavities.

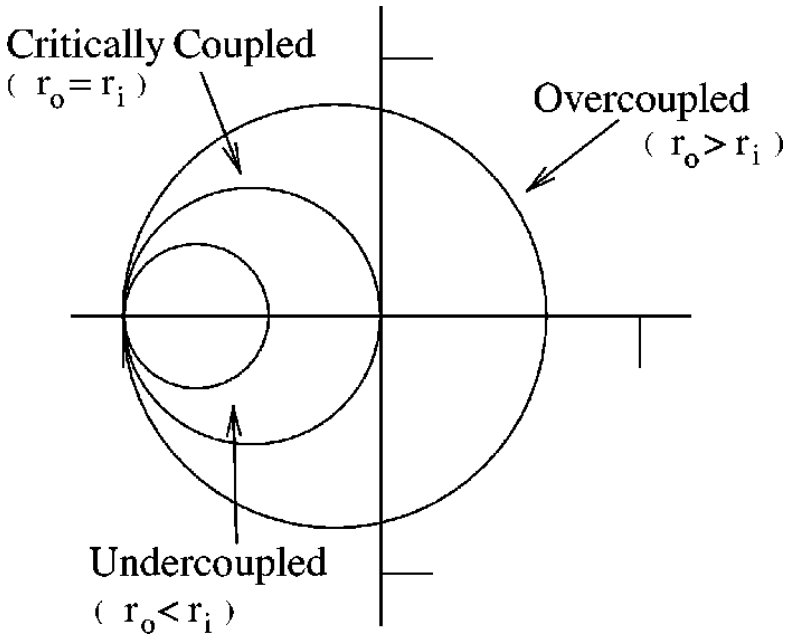

Fig. 11. The amplitude reflection coefficients for Fabry–Perot cavities are circles in the complex plane; r_i and r_o are the amplitude reflection coefficients of the input and output mirrors, respectively.

Amplitude ratio in the case of the Advanced Virgo mirrors.

$$\frac{E_{\text{reflected}}}{E_{\text{in}}} = \frac{-r_i + r_e(r_i^2 + t_i^2)e^{ik2L}}{1 - r_i r_e e^{ik2L}}$$

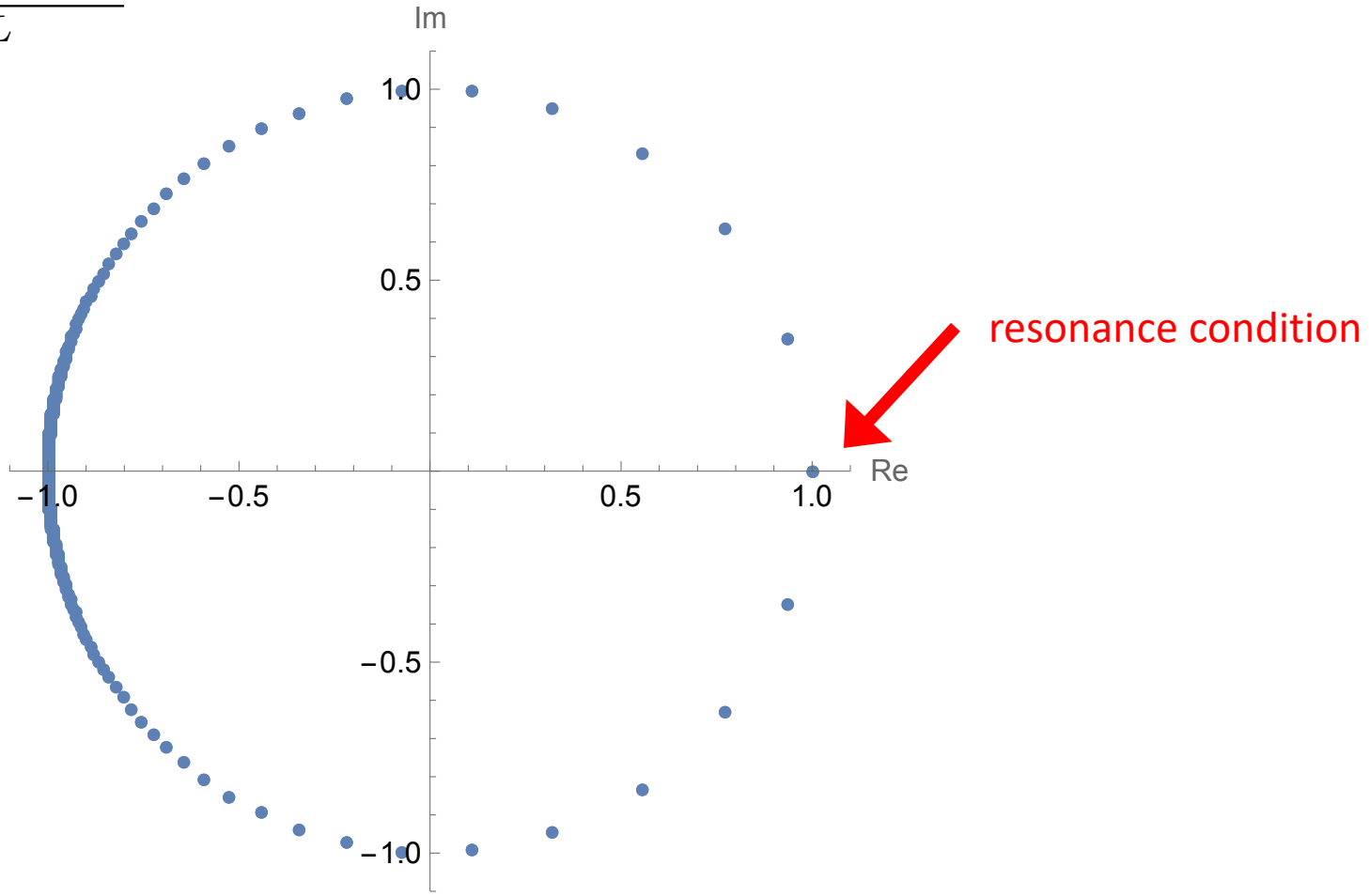

Following a length change in one arm

$$F = \frac{-r_i + r_e(r_i^2 + t_i^2)e^{ik2L}}{1 - r_i r_e e^{ik2L}} \quad \rightarrow \quad \frac{-r_i + r_e(r_i^2 + t_i^2)e^{ik2(L+\delta L)}}{1 - r_i r_e e^{ik2(L+\delta L)}}$$

Then, expanding about resonance, so that $e^{ik2L} = 1$ and $e^{ik2(L+\delta L)} = e^{ik2\delta L} \approx 1 + 2ik\delta L = 1 + \frac{4\pi i \delta L}{\lambda}$

$$F \approx \frac{-r_i + r_e(r_i^2 + t_i^2)(1 + 4\pi i\delta L/\lambda)}{1 - r_i r_e(1 + 4\pi i\delta L/\lambda)}$$

$$= \frac{-r_i + r_e(r_i^2 + t_i^2)(1 + 4\pi i\delta L/\lambda)}{(1 - r_i r_e) - 4\pi i r_i r_e \delta L/\lambda}$$

$$= \frac{-r_i + r_e(r_i^2 + t_i^2)(1 + 4\pi i\delta L/\lambda)}{1 - r_i r_e}\left(1 + \frac{4\pi i r_i r_e \delta L/\lambda}{1 - r_i r_e}\right)$$

$$\approx \frac{-r_i + r_e(r_i^2 + t_i^2)}{1 - r_i r_e} + \frac{8\pi i\delta L/\lambda}{1 - r_i r_e} \approx 1 + 8i\mathcal{F}\frac{\delta L}{\lambda}$$

When we include losses (e.g., due to mirror imperfections), we find the arm reflectances

$$r_{x,y} = \left(1 - \frac{\mathcal{F}}{\pi}\epsilon\right)\left(1 + 8i\mathcal{F}\frac{\delta L_{x,y}}{\lambda}\right)$$

average number of single passes inside cavity

average loss per single pass

This is the reflectance for the carrier.

For the sidebands we can assume that they are completely reflected by the input mirror with -1 amplitude reflectance.

The FP cavities act as individual mirrors, and their length is the same. The equivalent Michelson interferometer has arms that have only few meters, and the Schnupp asymmetry is applied to these short arms.

Close to resonance we find that the **full transfer function of the Michelson inteferometer with FP arms** is

- Carrier

$$
\begin{aligned}
H(\omega) &= \frac{1}{2}\left(r_x e^{ik(2\ell_x)} - r_y e^{ik(2\ell_y)}\right) \\
&\approx -\frac{1}{2}\left(1 - \frac{\mathcal{F}_{\rm ac}}{\pi}\epsilon\right)\left(e^{ik(2\ell_x)} - e^{ik(2\ell_y)} + 8i\mathcal{F}_{\rm ac}\frac{L}{\lambda}h e^{ik(2\ell_x)} + 8i\mathcal{F}_{\rm ac}\frac{L}{\lambda}h e^{ik(2\ell_y)}\right) \\
&= -\frac{1}{2}\left(1 - \frac{\mathcal{F}_{\rm ac}}{\pi}\epsilon\right) e^{ik(\ell_x+\ell_y)}\left(2i\sin k\delta\ell + 8i\mathcal{F}_{\rm ac}\frac{L}{\lambda}h\cos k\delta\ell\right) \\
&\approx -4ie^{ik(\ell_x+\ell_y)}\left(1 - \frac{\mathcal{F}_{\rm ac}}{\pi}\epsilon\right)\mathcal{F}_{\rm ac}\frac{L}{\lambda}h
\end{aligned}
$$

ac = arm cavity

use the Schnupp asymmetry here

- Sidebands

$$
\begin{aligned}
H(\omega_\pm) &= -ie^{ik_\pm(\ell_x+\ell_y)}\sin\left(\frac{(\omega \pm \Omega)\delta\ell}{c}\right) \\
&= \mp ie^{ik_\pm(\ell_x+\ell_y)}\sin\left(\frac{\Omega\delta\ell}{c}\right) \\
&= \mp ie^{ik_\pm(\ell_x+\ell_y)}\sin\left(2\pi\frac{\delta\ell}{\lambda_{\rm mod}}\right)
\end{aligned}
$$

use the Schnupp asymmetry here

Total electric field at the output port (Michelson interferometer with FP arms)

$$
\begin{aligned}
E_{\mathrm{out}} &= E_0 \left(H_0 J_0(\beta) e^{i\omega t} + H_+ J_1(\beta) e^{i(\omega+\Omega)t} - H_- J_1(\beta) e^{i(\omega-\Omega)t} \right) \\
&= -iE_{\mathrm{in}} e^{2ik\ell} \left[J_0(\beta) 4\mathcal{F}_{\mathrm{ac}} \frac{L}{\lambda} \left(1 - \frac{\mathcal{F}_{\mathrm{ac}}}{\pi} \epsilon \right) h + J_1(\beta) \sin\left(\frac{\Omega}{c} \delta\ell \right) \left(e^{i\Omega t + 2i\Omega\ell/c} + e^{-i\Omega t - 2i\Omega\ell/c} \right) \right] \\
&= -iE_{\mathrm{in}} e^{2ik\ell} \left[J_0(\beta) 4\mathcal{F}_{\mathrm{ac}} \frac{L}{\lambda} \left(1 - \frac{\mathcal{F}_{\mathrm{ac}}}{\pi} \epsilon \right) h + 2J_1(\beta) \sin\left(\frac{\Omega}{c} \delta\ell \right) \cos\left(\Omega t + 2\Omega\ell/c \right) \right]
\end{aligned}
$$

Total power at the output port

$$E_{\mathrm{out}} = -iE_{\mathrm{in}}e^{2ik\ell}\left[J_0(\beta)4\mathcal{F}_{\mathrm{ac}}\frac{L}{\lambda}\left(1-\frac{\mathcal{F}_{\mathrm{ac}}}{\pi}\epsilon\right)h + 2J_1(\beta)\sin\left(\frac{\Omega}{c}\delta\ell\right)\cos\left(\Omega t + 2\Omega\ell/c\right)\right]$$

$$\frac{P_{\mathrm{out}}(\Omega)}{P_{\mathrm{in}}} = 16J_0(\beta)J_1(\beta)\sin\left(\frac{\Omega}{c}\delta\ell\right)\mathcal{F}_{\mathrm{ac}}\frac{L}{\lambda}\left(1-\frac{\mathcal{F}_{\mathrm{ac}}}{\pi}\epsilon\right)h\cos\left(\Omega t + 2\Omega\ell/c\right)$$

$$V_{\mathrm{PD}}(\Omega) = 16(RP_{\mathrm{in}})J_0(\beta)J_1(\beta)\sin\left(\frac{\Omega}{c}\delta\ell\right)\mathcal{F}_{\mathrm{ac}}\frac{L}{\lambda}\left(1-\frac{\mathcal{F}_{\mathrm{ac}}}{\pi}\epsilon\right)h\cos\left(\Omega t + 2\Omega\ell/c\right)$$

$$V_{\mathrm{signal}} = 8(RP_{\mathrm{in}})J_0(\beta)J_1(\beta)\sin\left(\frac{\Omega}{c}\delta\ell\right)\mathcal{F}_{\mathrm{ac}}\frac{L}{\lambda}\left(1-\frac{\mathcal{F}_{\mathrm{ac}}}{\pi}\epsilon\right)h$$

Power recycling

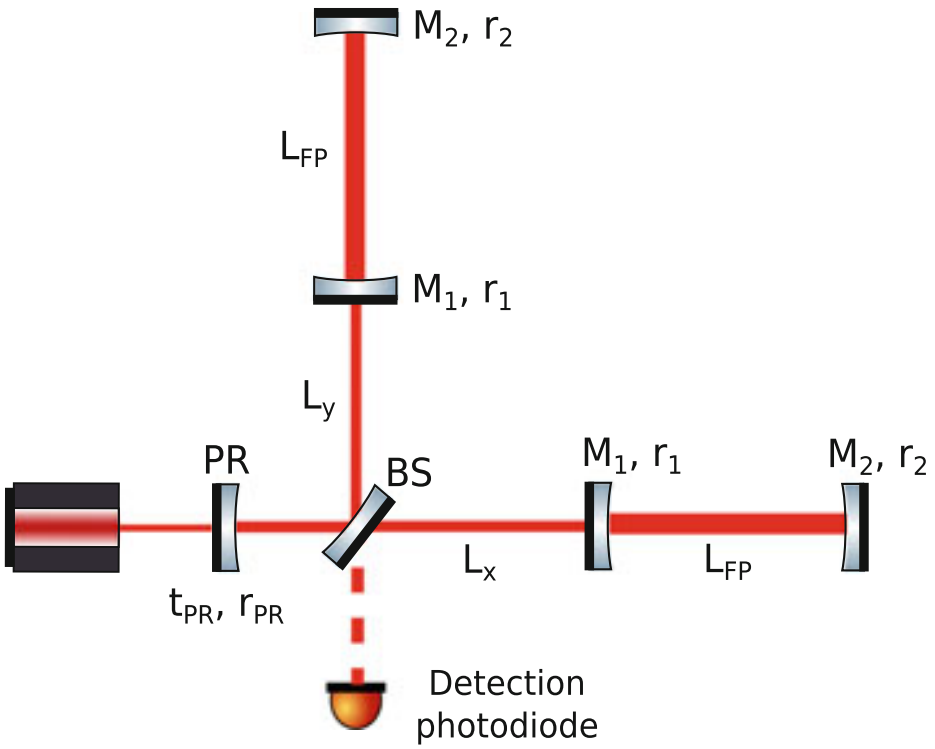

Scheme of a Michelson interferometer with Fabry Perot cavities in its arms and a power recycling mirror

Part of the power in the Michelson interferometer would head back towards the laser, and be lost.

The purpose of the power recycling cavity is that of making the power flow unidirectional, as in a standard FP cavity.

The recycling cavity acts as an additional FP cavity, where one of the mirrors is the power recycling mirror, and the other one is the whole interferometer with its FP arms.

In this case we wish to trasmit forward as much radiation as possible, while the backwards reflection should be as little as possible.

Clearly, the (amplitude) transmission coefficient of the cavity is

$$\frac{E_{\mathrm{transmitted}}}{E_{\mathrm{in}}} = \frac{t_i t_e e^{ikL}}{1 - r_i r_e e^{ik2L}} E_{\mathrm{in}} \quad \Rightarrow \quad t_{\mathrm{rc}} = \frac{t_{\mathrm{rm}} t_{\mathrm{ifo}} e^{ik\ell_{\mathrm{rm-bs}}}}{1 - r_{\mathrm{rm}} r_{\mathrm{ifo}} e^{ik2\ell_{\mathrm{rm-bs}}}}$$

where

- rc = recycling cavity
- ifo = interferometer
- bs = beam splitter
- rm = recycling mirror

Recycled power

Sidebands are off-resonance with respect to the F-P arm cavities, therefore $r_x = r_y = -1$, so that the reflectivity is given by the light going back to the symmetric port

$$r_{\rm ifo}^{(\pm)} = e^{ik_\pm(\ell_x+\ell_y)}\left(r_x e^{ik_\pm\delta\ell} + r_y e^{-ik_\pm\delta\ell}\right) = -e^{ik_\pm(\ell_x+\ell_y)}\left(e^{ik_\pm\delta\ell} + e^{-ik_\pm\delta\ell}\right)$$

$$= -e^{ik_\pm(\ell_x+\ell_y)}\cos\left(k_\pm\delta\ell\right) = -e^{ik_\pm(\ell_x+\ell_y)}\cos\left(k\delta\ell \pm \frac{\Omega}{c}\delta\ell\right)$$

$$= -e^{ik_\pm(\ell_x+\ell_y)}\left[\cos k\delta\ell\ \cos\left(\frac{\Omega}{c}\delta\ell\right) \mp \sin k\delta\ell\ \sin\left(\frac{\Omega}{c}\delta\ell\right)\right]$$

$$= -e^{ik_\pm(\ell_x+\ell_y)}\cos\left(\frac{\Omega}{c}\delta\ell\right)$$

use the Schnupp asymmetry here

while the interferometer transmission coefficient represents light moving towards the antisymmetric port, and corresponds to the transfer function that we have just found

$$t_{\rm ifo}^{(\pm)} = \mp i e^{ik_\pm(\ell_x+\ell_y)}\sin\left(2\pi\frac{\delta\ell}{\lambda_{\rm mod}}\right)$$

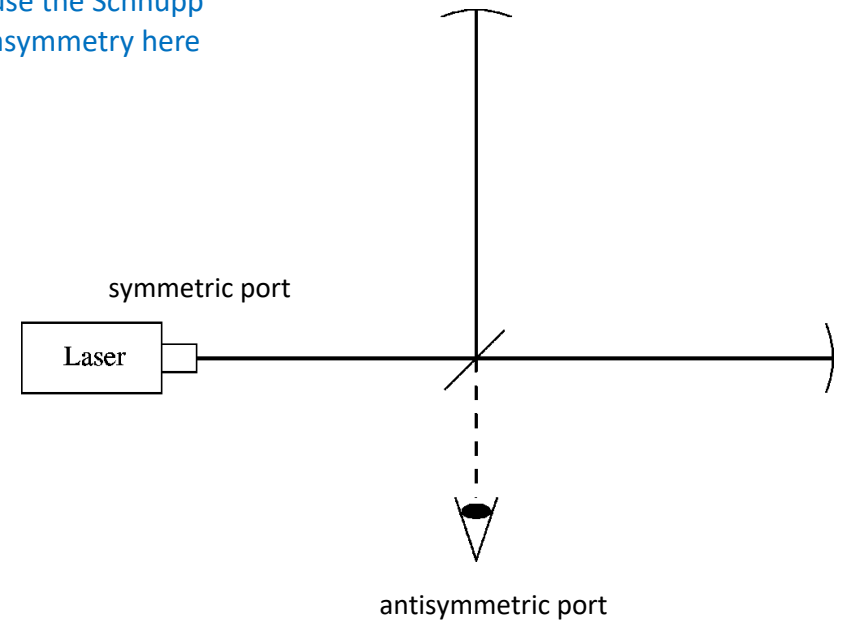

Using these values

$$r_{\mathrm{ifo}}^{(\pm)} = -e^{ik_{\pm}(\ell_x+\ell_y)} \cos\left(2\pi \frac{\delta\ell}{\lambda_{\mathrm{mod}}}\right)$$
$$t_{\mathrm{ifo}}^{(\pm)} = \mp i e^{ik_{\pm}(\ell_x+\ell_y)} \sin\left(2\pi \frac{\delta\ell}{\lambda_{\mathrm{mod}}}\right)$$

we find the reflection coefficient of the power recycling cavity

$$\frac{E_{\mathrm{reflected}}}{E_{\mathrm{in}}} = \frac{-r_{\mathrm{rm}} + r_{\mathrm{ifo}}(r_{\mathrm{rm}}^2 + t_{\mathrm{rm}}^2)e^{ik2\ell_{\mathrm{rm-bs}}}}{1 - r_{\mathrm{rm}} r_{\mathrm{ifo}} e^{ik2\ell_{\mathrm{rm-bs}}}}$$

from which – after substitution of the ifo values – we see that the resonance condition is

$$e^{ik_{\pm}(\ell_x+\ell_y+2\ell_{\mathrm{rm-bs}})} = -1$$

and that the reflected field vanishes for

$$\cos\left(2\pi \frac{\delta\ell}{\lambda_{\mathrm{mod}}}\right) = r_{\mathrm{rm}}$$

which requires an adjustment of the Schnupp asymmetry to satisfy this constraint as well.

On the whole, on resonance there is no reflection and the transmission coefficient for sidebands is

$$t_{\mathrm{rc}} = \frac{t_{\mathrm{rm}} t_{\mathrm{ifo}} e^{ik_{\pm}\ell_{\mathrm{rm-bs}}}}{1 - r_{\mathrm{rm}} r_{\mathrm{ifo}} e^{ik_{\pm}2\ell_{\mathrm{rm-bs}}}} \;\rightarrow\; \pm i e^{-ik_{\pm}l_{\mathrm{rm-bs}}}$$

Similar calculations can be carried out for the carrier beam and one finally finds the transfer function of the complete interferometer

$$H(\omega) = i e^{-ik\ell_{\mathrm{rm-bs}}} \frac{4}{\sqrt{\pi}} \mathcal{F}_{\mathrm{ac}} \sqrt{\mathcal{F}_{\mathrm{rc}}} \frac{L}{\lambda} h$$

So that the voltage signal at the end of the detection chain is

$$V_{\mathrm{signal}} = \frac{4}{\pi} (R P_{\mathrm{in}}) J_0(\beta) J_1(\beta) \mathcal{F}_{\mathrm{ac}} \sqrt{\mathcal{F}_{\mathrm{rc}}} \frac{L}{\lambda} h$$

Power recycling

The complete setup of the power recycling system must take into account that:

- The carrier field must be on resonance in the arm Fabry-Perot cavities
- The carrier field must be on resonance in the power recycling cavity to enhance the effective input power as much as possible
- The arm FP stabilization feedback uses the sidebands as phase reference; for this reason, the sidebands must be off-resonance in the arm cavities and reflect off the input mirrors of the arm FPs
- The sidebands must be on resonance in the power recycling cavity, otherwise, they would not reach the input mirrors of the arm FPs
- A phase reference is also needed to build up an error signal for power recycling cavity; for this reason, it is necessary to use a modulation frequency that is not resonant in the power recycling cavity
- **the power recycling cavity of Virgo needs a special consideration due to its optical configuration which is very close to the limit of stability since $1 - g_1 g_2 = 0.19 \times 10^{-5}$.**

The consequence of being so close to the instability region is that the frequencies of the HOMs (Higher order modes) are very close to the fundamental mode. In this case, HOMs – due, for example to misalignment or mismatch – will couple very strongly to the optical cavity, diminishing power in the fundamental mode.

The frequency separation between HOMs in the power recycling cavity of Virgo is 11.3 kHz. When compared to the linewidth which is 210 kHz it is obvious that HOMs are very relevant.

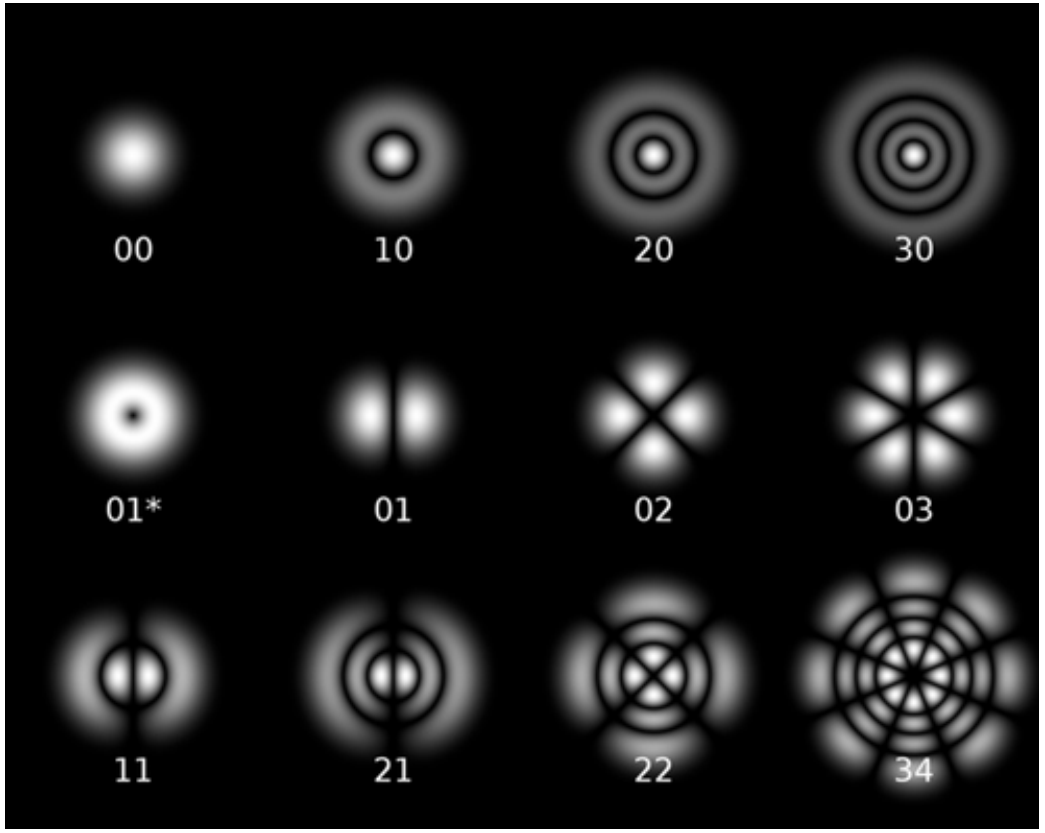

The spatial intensity profiles of Laguerre-Gaussian modes.

The complete scheme includes a signal recycling cavity as well

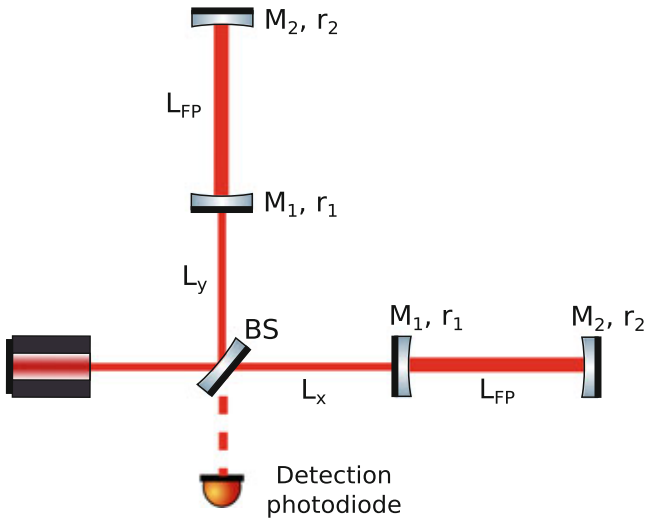

Scheme of a Michelson interferometer with Fabry-Perot cavities on its arms

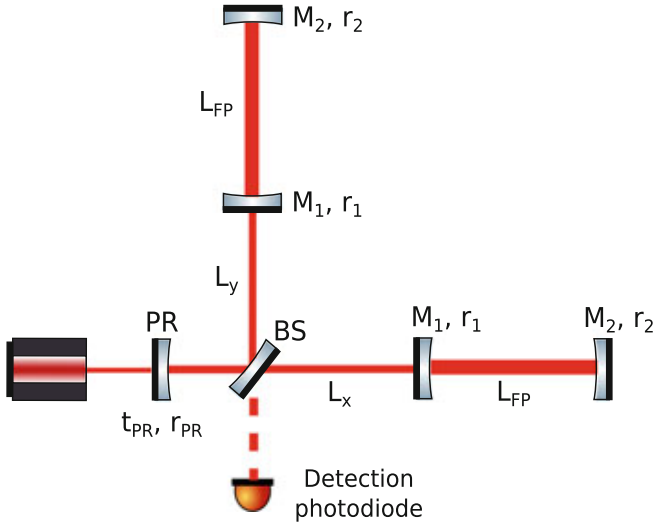

Scheme of a Michelson interferometer with Fabry Perot cavities on its arms and a power recycling mirror

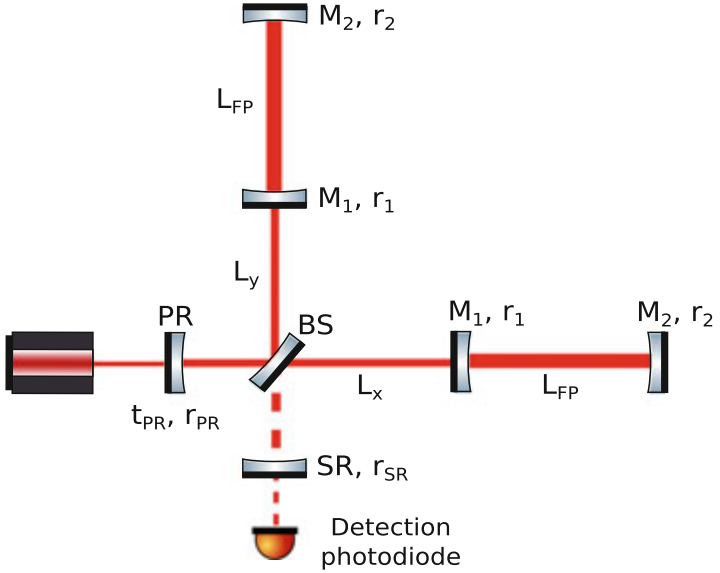

Scheme of a Michelson interferometer with Fabry Perot cavities on its arms, a power recycling mirror and a signal recycling mirror

Advanced Virgo

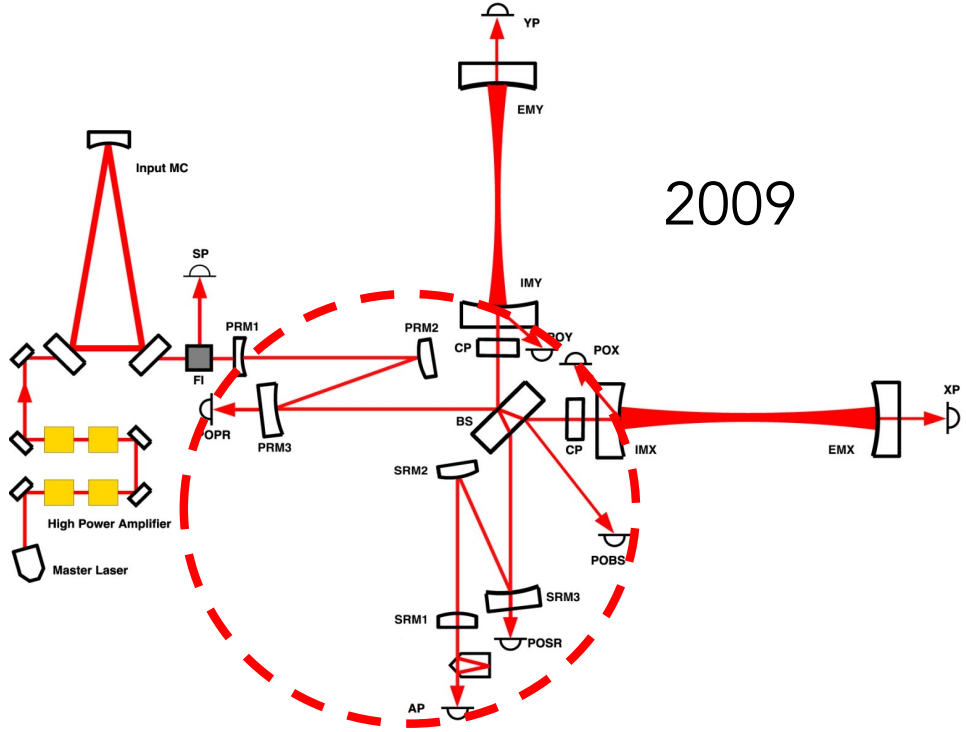

2009

2011

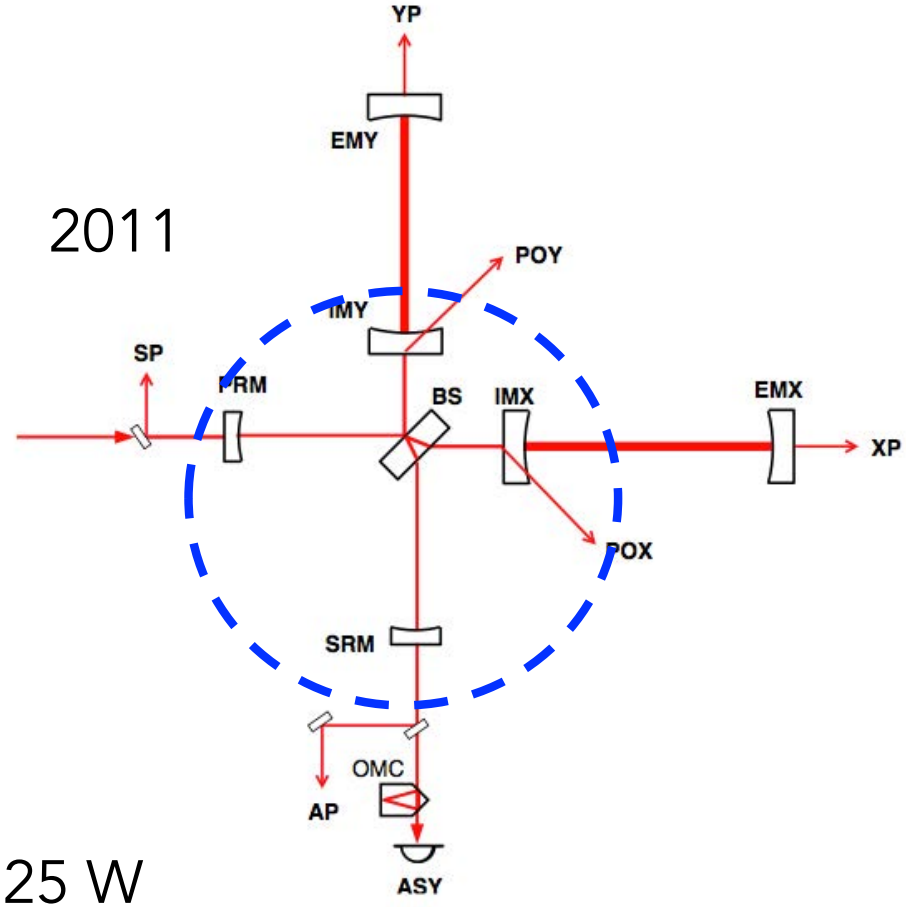

Target input power: 125 W

There is much more to the current advanced interferometers, but in this introductory course we stop here.

If you wish to know more, a good reference is the published PhD thesis of Julia Casanueva Diaz (link).

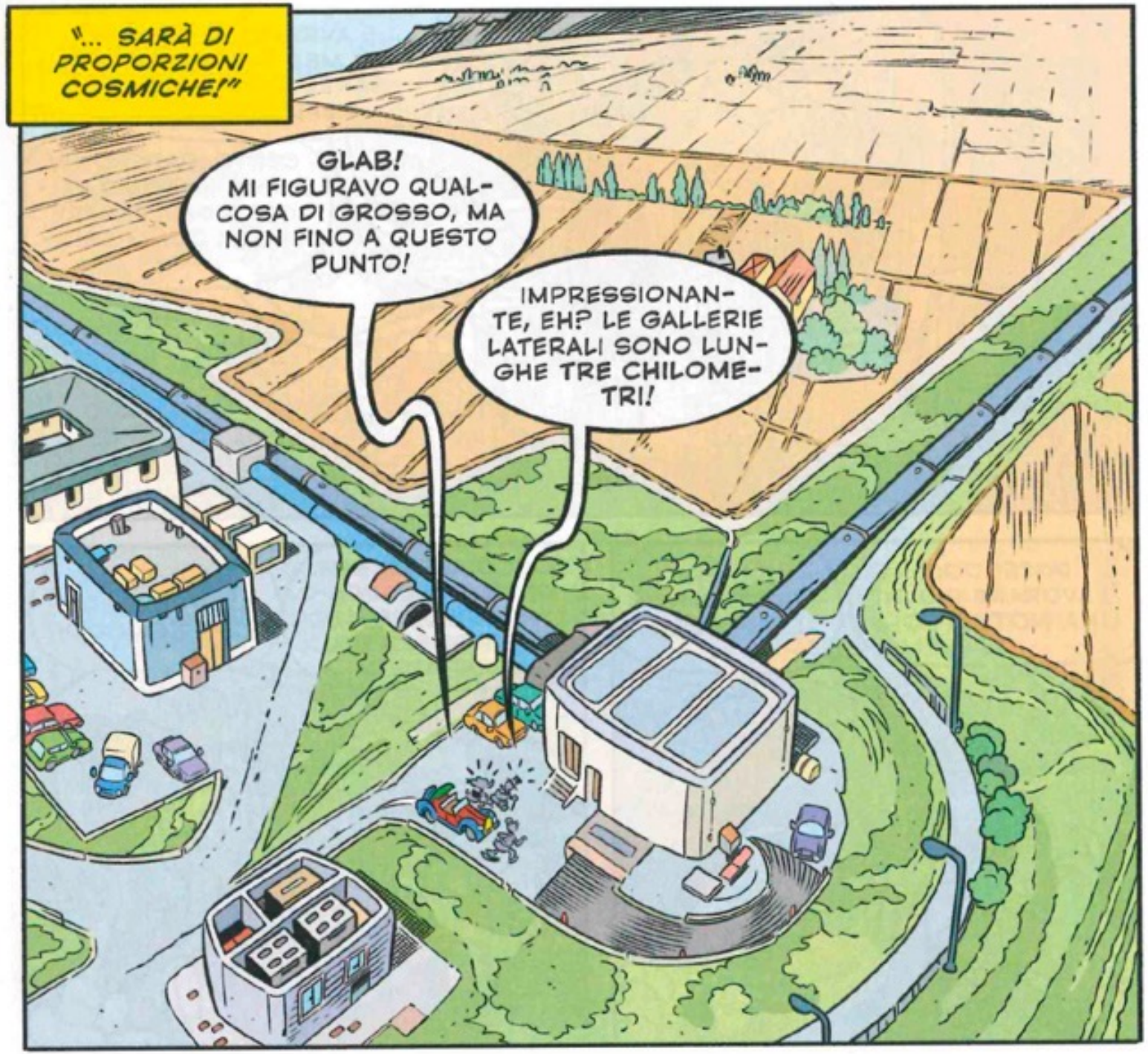
"... SARÀ DI PROPORZIONI COSMICHE!"
GLAB! MI FIGURAVO QUALCOSA DI GROSSO, MA NON FINO A QUESTO PUNTO!
IMPRESSIONANTE, EH? LE GALLERIE LATERALI SONO LUNGHE TRE CHILOMETRI!

Differential equation satisfied by the generating function of the Bessel functions

Starting from

$$x^2 \frac{\partial^2 J_n}{\partial x^2} + x \frac{\partial J_n}{\partial x} + \left(x^2 - n^2\right) J_n = 0$$

after multiplying throughout times t^n and summing over n, we see at once that this is leads to

$$x^2 \frac{\partial^2 F}{\partial x^2} + x \frac{\partial F}{\partial x} + x^2 F = \sum_{n=-\infty}^{+\infty} n^2 t^n J_n(x)$$

and the sum can be rearranged as follows

$$\begin{aligned} \sum_{n=-\infty}^{+\infty} n^2 t^n J_n(x) &= t \sum_{n=-\infty}^{+\infty} n \left(\frac{\partial}{\partial t} t^n \right) J_n(x) = t \frac{\partial}{\partial t} \sum_{n=-\infty}^{+\infty} n t^n J_n(x) \\ &= t \frac{\partial}{\partial t} t \frac{\partial}{\partial t} \sum_{n=-\infty}^{+\infty} n t^n J_n(x) = t \frac{\partial}{\partial t} t \frac{\partial F}{\partial t} \\ &= t^2 \frac{\partial^2 F}{\partial t^2} + t \frac{\partial F}{\partial t} \end{aligned}$$

and this concludes the proof.